Solvation Effects on Reactive Intermediates: The Benzyl Radical and Its Clusters with Ar, N2, CH4, C2H6, and C3H8

ARTICLE *in* THE JOURNAL OF CHEMICAL PHYSICS · MARCH 1993

Impact Factor: 2.95 · DOI: 10.1063/1.464996

2 AUTHORS:

Robert S. Disselkamp
Solis Research
68 PUBLICATIONS **845** CITATIONS
SEE PROFILE

Elliot R Bernstein
Colorado State University
317 PUBLICATIONS **6,921** CITATIONS
SEE PROFILE

SECURITY CLASSIFICATION OF T...

REPORT DOCUMENTATION PAGE

Form Approved
OMB No 0704-0188

1a REPORT SECURITY CLASSIFICATION	1b. RESTRICTIVE MARKINGS
2a SECURITY CLASSIFICATION AUTHORITY	3. DISTRIBUTION / AVAILABILITY OF REPORT Aporoved for public release; distribution unlimited.
2b DECLASSIFICATION / DOWNGRADING SCHEDULE Unclassified	
4 PERFORMING ORGANIZATION REPORT NUMBER(S) N00014-89-J-1237	5. MONITORING ORGANIZATION REPORT NUMBER(S)
6a NAME OF PERFORMING ORGANIZATION Colorado State University	6b. OFFICE SYMBOL (If applicable)
6c ADDRESS (City, State, and ZIP Code) Department of Chemistry Fort Collins, CO 80523	7a. NAME OF MONITORING ORGANIZATION 7b. ADDRESS (City, State, and ZIP Code)
8a NAME OF FUNDING / SPONSORING ORGANIZATION Office of Naval Research	8b. OFFICE SYMBOL (If applicable)
8c ADDRESS (City, State, and ZIP Code) 800 North Quincy Street Arlington, VA 22217-5000	9. PROCUREMENT INSTRUMENT IDENTIFICATION NUMBER N00014-89-J-1237
	10. SOURCE OF FUNDING NUMBERS PROGRAM ELEMENT NO / PROJECT NO / TASK NO / WORK UNIT ACCESSION NO

11 TITLE (Include Security Classification)
Solvation Effects on Reactive Intermediates: the Benzyl Radical and Its Clusters with Ar, N_2, CH_4, C_2H_6, and C_3H_8

12 PERSONAL AUTHOR(S)
R. Disselkamp and E. R. Bernstein

13a TYPE OF REPORT	13b. TIME COVERED	14. DATE OF REPORT (Year, Month, Day)	15 PAGE COUNT
Technical Report	FROM _____ TO _____	December 11, 1992	

16 SUPPLEMENTARY NOTATION

17 COSATI CODES			18. SUBJECT TERMS (Continue on reverse if necessary and identify by block number)
FIELD	GROUP	SUB-GROUP	mass resolved excitation spectra, red shifts, electronic transition region, electronic states, van der Waal modes, vibronic coupling, transition energies, ionization energy

19 ABSTRACT (Continue on reverse if necessary and identify by block number)

SEE ATTACHED ABSTRACT

20 DISTRIBUTION / AVAILABILITY OF ABSTRACT	21. ABSTRACT SECURITY CLASSIFICATION
☒ UNCLASSIFIED/UNLIMITED ☐ SAME AS RPT. ☐ DTIC USERS	Unclassified
22a NAME OF RESPONSIBLE INDIVIDUAL Elliot R. Bernstein	22b. TELEPHONE (Include Area Code) (303) 491-6347
	22c OFFICE SYMBOL

DD Form 1473, JUN 86 — Previous editions are obsolete. — SECURITY CLASSIFICATION OF THIS PAGE

S/N 0102-LF-014-6603

OFFICE OF NAVAL RESEARCH

Contract N00014-89-J-1237

TECHNICAL REPORT #82

Solvation Effects on Reactive Intermediates: the Benzyl Radical and Its Clusters with Ar, N_2, CH_4, C_2H_6, and C_3H_8

by

R. Disselkamp and E. R. Bernstein

Accepted by

Journal of Chemical Physics

Department of Chemistry
Colorado State University
Fort Collins, Colorado 80523

November 4, 1992

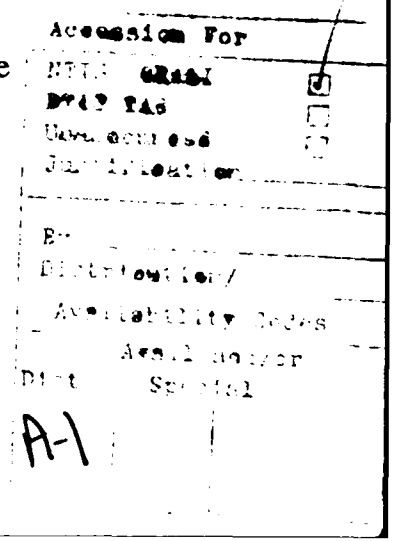

ABSTRACT

Mass resolved excitation spectra are presented for the benzyl radical and its clusters with Ar, N_2, CH_4, C_2H_6, and C_3H_8. The cluster spectra exhibit small red shifts (< 50 cm^{-1}) relative to the unclustered benzyl radical for the $D_1(1^2A_2) \leftarrow D_0(1^2B_2)$ and $D_2(2^2B_2) \leftarrow D_0(1^2B_2)$ electronic transition regions. A unique set of low energy van der Waals modes is observed for these clusters for each excited electronic state investigated. The cluster spectra also reveal significant vibronic coupling between the two excited electronic states of the benzyl radical, as evidenced by a single vibrational predissociation threshold for each cluster. Ab initio calculations are performed on the benzyl radical to examine excited electronic state structure, predict transition energies, estimate ionization energy, and determine partial atomic charges in the electronic states of interest. The resulting partial charges are used in empirical atom-atom potential energy calculations to aid in the understanding of cluster spectroscopic shifts, binding energies, and van der Waals modes.

I. INTRODUCTION

Most of the spectroscopic information on reactive intermediates accrues from either matrix isolation[1-5] or room temperature gas phase[6-8] experimental studies. Within the last ten years, however, studies of reaction intermediates, in particular radicals, have been reported employing supersonic jet expansion techniques.[9-12] These recent radical generation techniques involve either electric discharge, photolysis, or thermal decomposition of suitable precursors, occurring as part of the supersonic expansion. When such techniques are combined with fluorescence, mass resolved excitation, or dispersed fluorescence detection, very detailed information can be obtained concerning the ground and excited state properties of radicals.

Over the past 35 years the benzyl radical has been the subject of many experimental[9-23] and theoretical studies.[24-32] The benzyl radical is a simple aromatic stabilized π radical with relatively high symmetry (C_{2v}). Early theoretical calculations correctly predict the ground state to have $^2B_2$ symmetry, but disagree as to the ordering of the 1^2A_2 and 2^2B_2 first two excited states. This theoretical uncertainty as to the ordering of the excited states is understandable considering their close proximity. (It is now known that the 2^2B_2 state lies roughly 400 cm^{-1}, or 0.05 e V, above the 1^2A_2 state.) Experimental work conducted by Leach and co-workers[18] reveals that a low lying first excited (D_1) state of $^2A_2$ symmetry lies at 22,000 cm^{-1}. Their determination of the D_1 excited state symmetry relies on a rotational band contour analysis of the emission spectra of several deuterated benzyl radical species. This assignment was later confirmed by Friedricht et.al.[17] An inspection of the benzyl radical absorption and emission data reveals the existence of three intense features between 300-650 cm^{-1} above the assigned 1^2A_2 electronic origin with no readily identifiable comparable features accessible in the ground state. Cossart-Magos and Leach[19] performed a linear pseudo-Jahn-Teller (LPJT) vibronic coupling calculation which treats the interaction between the $18b^1$ and $6b^1$ vibrations of the 1^2A_2 electronic state with the 2^2B_2 electronic state. Their calculations, which account for the experimentally observed isotope effects, predict the unperturbed 2^2B_2 electronic origin to lie roughly 400 cm^{-1} above the 1^2A_2 origin. More refined vibronic coupling calculations have been performed[25,26] which include the $8b^1$, in

addition to the $18b^1$ and $6b^1$ vibrations. These reanalyses of the problem predict the unperturbed 2^2B_2 electronic state to be ~850 cm^{-1} above the 1^2A_2 electronic state. Recently, well resolved supersonic jet generated spectra of the benzyl radical have been obtained using time-of-flight mass resolved,[9] and dispersed emission[11] (DE) experimental techniques which confirm the location of these vibronic features.

Although radicals are known to play an important role as reaction intermediates in condensed phases,[33] little is understood about their solvation physics and chemistry. Here we report a study of the effect of solvation by non-polar molecules on the electronic transitions of the benzyl radical. Many of the phenomena observed for the radical solute-solvent clusters examined here (e.g., small spectroscopic red shifts, appearance of van der Waals vibrational modes in the cluster spectra, vibrational predissociation, vibronic coupling) are known to be important for clusters of stable species.

The experimental results presented in this report include cluster transition energy shifts with respect to the bare radical, an estimation of cluster binding energy for different radical electronic states, and an identification of cluster vibrational/torsional van der Waals structure. Calculations of benzyl radical electronic states, cluster structure, and binding energies are employed to aid in the elucidation of the experiment results. In particular, ab initio calculations are performed to examine electronic state structure and to determine atomic partial charges in the ground and first two excited electronic states. These partial charges are used in conjunction with dispersion and repulsion atom-atom interaction parameters to estimate cluster structure, binding energy, and vibrational/torsional van der Waals motion.

II. PROCEDURES

1 Experiments

Experiments based on the generation and detection of radicals are similar to those of stable species performed previously in this laboratory,[34] although subtle differences are encountered in

studying the two types of samples. What follows is a discussion of these differences as well as a detailed description of the formation and detection of the benzyl radical and its clusters.

Figures 1 and 2 pictorially represent the optical and electronics configuration used in our experimental study of radicals. Figure 1 schematically illustrates the generation and detection of radicals. An ArF excimer laser with an output power of roughly 80 mJ/pulse was focused onto the exit region of an R.M Jordan pulsed valve operating at 10 Hz. Helium was used as the expansion gas at a backing pressure of 80 pisg and clusters were formed by using an expansion mixture containing 10% of the clustering agent of interest. The radicals and their clusters generated in the high density photolysis region are collisionally cooled and travel downstream to a pair of ion extraction plates (flight time roughly 50μs) where they were optically excited to a particular vibronic state of D_1 or D_2 and ionized by the absorption of a second photon. The ions created were extracted by a 350 V potential difference and accelerated into a time-of-flight mass spectrometer by ~4 keV. Mass resolved detection of the ionized radical species was accomplished via a Galieo Electro-Optics multi-channel-plate (MCP) detector at the end of a 1.5 m flight tube, generating mass resolved excitation spectra (MRES). For the systems presently under study, two Nd:YAG pumped dye lasers were used as the excitation and ionization source. Either C460 or C440 was used as the dye lasing medium for the $D_1,D_2 \leftarrow D_0$ excitation source and F548 (frequency doubled) was used as the dye lasing medium for the $I \leftarrow D_1,D_2$ ionization source.

The configuration of electronic instruments needed to control the timing of the above events is schematically illustrated in Figure 2. A trigger pulse originating from the oscillator of laser 1 was sent to the oscillator of laser 2 such that the Q-switches of lasers 1 and 2 were activated simultaneously. This "common" oscillator trigger was also passed through a delay stage and used to trigger the pulsed valve power supply. The output trigger from the pulsed valve power supply was then sent to another delay stage and used to activate the ArF excimer laser. Detection of the radicals was achieved by sending the variable synch trigger of laser 1 to a Stanford-Research-System (SRS) delay box which controls both the boxcar averager/oscilloscope timing and the data acquisition peripherals. Since the firing of the excimer laser created a 0.9 V RF noise pulse

transmitted through our detection electronics, the input threshold on the SRS instrument was set at greater than 1.0 V. To alleviate additional grounding and feedback problems, an opto-isolator was placed between the Q-switch of laser 2 and the electronics of the wavelength extension system (WEX) in order to amplify the triggering pulse.

The next step taken in achieving benzyl radical signal was to align (spatially and temporally) the excitation laser, ionization laser, and photolysis laser. This is accomplished through a four step procedure. First, the excimer laser output (193 nm) was spatially aligned by removing the back plate of the vacuum chamber and focusing the light beam to a spot size of 5 mm^2 onto the exit region of the nozzle. Second, the output from the excitation and ionization lasers was reduced in intensity and focused onto a fast photodiode (EG&G FND100 reversed biased by 15 V, response time <5ns) with the signal output sent to an oscilloscope. This allowed a temporal overlap of the two laser pulses to be achieved. Third, a one color mass detected aniline signal (at roughly 36,400 cm^{-1}) was used to optimize the nozzle delay and spatial alignment of the ionization laser. The aniline signal was also used as a check of mass calibration. Finally, the excimer laser was temporally aligned while monitoring the one-color aniline signal: at a unique time delay the firing of the excimer resulted in a decrease of the observed aniline signal by more than a factor of 10. This signal decrease is attributed to photolysis of aniline (possibly multiphoton) into unknown products. Since the only remaining degree of freedom in the experimental set-up was the spatial alignment of the excitation laser, the benzyl radical signal could be readily found. During optimum operation, 2 V of benzyl radical signal was obtained, with cluster signals varying from 30 mV to 400 mV. Benzyl chloride (stated purity 99%), purchased from Aldrich Chemical Company, was used as the benzyl radical precursor. Negative peaks in the observed spectra depicted in the figures result from detector overload due to intense signals in lower mass channels.

2. Ab initio Calculations

In order to analyze and understand the benzyl radical cluster spectra discussed here we perform ab initio calculations to explore the effect of electronic excitation on the benzyl radical. We

are particularly interested in determining the electronic charge distribution in the ground and first two excited electronic states. Calculations are carried out using the HONDO[35] molecular orbital package running on an IBM risc/6000 computer system equipped with 1.5 GB of storage space and 64 MB of RAM. Complete-active-space-self-consistent-field (CASSCF) calculations using the Dunning-Huzinaga [9s,5p]/[3s/2p] double zeta-valence basis set (DZV) are performed on the ground and first two excited electronic states of the benzyl radical. The active space consists of benzyl radical π orbitals: this restriction results in 404 electronic configurations for states of B_2 symmetry and 380 configurations for states of A_2 symmetry. A geometry optimization was performed for each of the elctronic states by reducing energy gradients to less than 10^{-4} a.u.

The calculations presented here are similar to calculations performed by Rice, et al.[24] who chose the same calculational approach but different basis sets: a full double zeta (DZ) basis, and a full double zeta basis plus polarization and diffuse functions on the carbon atoms (DZd+). Their DZ results for the three lowest electronic states of the benzyl radical are lower in energy than our DZV results by less than 0.0005 a.u. The DZd+ basis set results give rise to only a slight improvement in $1^2A_2 \leftarrow 1^2B_2$ transistion energy. Since the addition of polarization functions is shown not to increase the accuracy of calculated partial atomic charges for small molecules comprised only of carbon and hydrogen, such as CH_4, C_2H_2, and C_2H_4,[36,37] we have opted to use the DZV results to determine benzyl radical partial charges. The general procedure for obtaining partial atomic charges has recently been extended to larger systems and excited states.[38] What follows is a brief description of our method of obtaining partial charges.

The general method used to estimate partial charges for a molecule involves creating a 3-dimensional map of the electrostatic potential for the electronic state of interest and numerically fitting charges centered at the atomic positions to this potential. The particular method we use is similar to that of Williams et al.[36] First, the electrostatic potential is evaluated at specific grid points. The grid chosen is a simple 3-dimensional cubic grid with a spacing of 2.0 bohr between points. The total grid size is made sufficiently large to encompass the entire molecule and extend well beyond the van der Waals radius of the molecule. Second, the electrostatic potential points

used to determine the partial charges are chosen by requiring that they lie outside the van der Waals radii of all the atoms and within a certain "shell thickness". The van der Waals radii used are[39,40] R_{vdw}(Carbon)=3.884 bohr and R_{vdw}(Hydrogen)=3.184 bohr. A shell thickness of 4.0 bohr is employed for these calculations.[36] This value is chosen to maximize the number of points for the determination of charges, while simultaneously minimizing the errors introduced by assuming each point has equal weight. Third, a standard non-linear fitting routine is employed to obtain the final values of the charges[41] by setting the magnitude of the error in each point equal to its value.

Concern has been expressed in the literature about the type of grid chosen (i.e., cubic, elliptical, etc.).[38] For example, when benzene's partial charges are determined using a cubic grid, a large discrepancy between the charges on carbon atoms and hydrogen atoms is found: a 4 to 2 "split" in the carbon (and hydrogen) charges is observed.[38] While we observe similar results using various grid spacings and shell thicknesses, our parameters above for benzene yield a minimal 4 to 2 split for the carbon partial atomic charges: carbons 2, 3, 5, and 6 have partial atomic charges of -0.160 electrons and carbons 1 and 4 have partial atomic charges of -0.162 electrons. The hydrogen charges are such that the individual C–H fragments have zero overall charge. For methane, we calculate hydrogen partial charges of +0.138 electrons, consistent with earlier studies.[39] While a more efficient method of generating electrostatic grid points is advantageous,[38] the straightforward approach employed here has been shown to accurately predict electric multipole properties.[36,37]

3. Empirical Atom-Atom Potential Energy Calculations

Atomic partial charges for the benzyl radical in the ground and excited states can be used in conjunction with van der Waals parameters to estimate benzyl radical binding energy with the solvents Ar, N_2, CH_4, C_2H_6, and C_3H_8. Non-bonded intramolecular interactions can be approximated by an atom-atom pair potential function consisting of a van der Waals exponential-6 potential term and an electrostatic partial charge interaction such as[40]

$$V_{BE} = \Sigma_{i,j>i} V_{ij} = A_{ij}\exp(-B_{ij}R_{ij}) - C_{ij}/R_{ij}^{6} + 116200\, Q_iQ_j/R_{ij} = V_{vdW} + V_c \qquad (1)$$

in which R_{ij} in Å is the separation distance between atoms i and j on different molecules, A_{ij}, B_{ij}, and C_{ij} are van der Waals parameters, and Q_i, Q_j in units of electron charge are the atomic partial charges. The numerical constant in Eq. (1) is a unit conversion factor to wavenumbers. Table I lists values of the van der Waals parameters used in this study. For interactions between different atomic species, A_{ij} and C_{ij} are obtained from the geometric mean of the homonuclear interaction terms, whereas B_{ij} is obtained from the arithmetic mean. The geometry of the benzyl radical is chosen as the 1^2B_2 CASSCF optimized structure, and experimentally determined geometries are used for the solvents.[42] All solvent hydrogen partial charges are taken as 0.14 e^- with negative charges equally distributed among the carbon atoms so as to generate a zero net molecular charge.[39] Charges on the nitrogen molecule are placed on the nitrogen atom sites (+0.377 e^-) and 0.25 Å away from the end of each nitrogen atom (i.e., lone-pair charges) on the molecular axis (-0.377 e^-).[43] This distribution of charge reproduces the known nitrogen quadrupole moment.[44] Cluster energies are minimized assuming rigid solvent and solute species using the SIMPLEX technique.[41]

III. RESULTS AND DISCUSSION

1. Benzyl Radical

The 2-color MRES of the benzyl radical is presented in Figure 3.[9] The spectrum contains an origin for the $D_1 \leftarrow D_0$ ($1^2A_2 \leftarrow 1^2B_2$) transition at 21,996 cm^{-1}, intense features 300-650 cm^{-1} to the blue of this origin arising in part from $1^2A_2 — 2^2B_2$ vibronic coupling, and a rather dense collection of transitions to higher energy. Summarizing the analysis of Cossart-Magos and Leach,[19] the two features labeled A_1 and A_3 correspond to vibronic features of roughly an equal hybrid of the 2^2B_2 electronic state origin and the $6b^1$ vibration of the 1^2A_2 electronic state. The feature labeled A_2 is believed to be the $18b^1$ vibration of the 1^2A_2 electronic state which remains essentially unchanged in energy, but borrows intensity from the 2^2B_2 electronic state. The labeled feature of least intensity in this region is the totally symmetric $6a^1$ vibration built on the 1^2A_2

electronic state origin (0_0^0). We will comment further on these assignments after analyzing spectra of the benzyl radical clusters.

Table II contains results of ab initio calculations for the benzyl radical. The ground and first two excited states are calculated. A CASSCF calculation using the Dunning-Huzinaga [9s, 5p]/[3s,2p] DZV basis set predicts the incorrect excited electronic state 1^2A_2 — 2^2B_2 ordering by roughly 1000 cm^{-1}. The transition energies to these states are accurately estimated to within roughly 1000 cm^{-1} of those observed. Table II shows that geometry relaxation lowers the excited state energies by 0.07 a.u., but has little effect on the ground state energy. The active space for these calculations consisted of the seven valence π-orbitals of the aromatic system. The major electronic configurations contributing to the three states of interest are found to be: 1^2B_2 state - $(b_2)^2\,(b_2)^2\,(a_2)^2\,(b_2)^1\,(a_2)\,(b_2)\,(b_2)$ 50%, 1^2A_2 state - $(b_2)^2\,(b_2)^2\,(a_2)^2\,(a_2)^1\,(b_2)\,(b_2)\,(b_2)$ 31%, $(b_2)^2\,(b_2)^2\,(a_2)^1\,(a_2)\,(b_2)^2\,(b_2)\,(b_2)$ 22%; and 2^2B_2 state - $(b_2)^2\,(b_2)^1\,(a_2)^2\,(b_2)^2\,(a_2)\,(b_2)\,(b_2)$ 23%, and $(b_2)^2\,(b_2)^2\,(a_2)^2\,(b_2)\,(a_2)\,(b_2)^1\,(b_2)$ 29%. Other electronic configurations (for each electronic state) contribute less than 13% to each the of the states. Also listed in the bottom portion of Table II is the calculated ionization energy. The calculated value of 59,210 cm^{-1} is in reasonable agreement with our measured value of 58,358 cm^{-1}.[9] In spite of the calculation's inability to predict the correct state ordering, accurate estimation of transition and ionization energies is encouraging.

As described in the last section, ab initio calculations can be used to generate atomic partial charges. Accurate atomic partial charges are necessary when evaluating the intermolecular van der Waals potential (e.g., Lennard-Jones-Coulomb, and exponential-6-Coulomb potentials). Table III lists the results of the partial charge calculations for the benzyl radical in its 1^2B_2, 1^2A_2, and 2^2B_2 electronic states. Listed in the final column of this table is the calculated residual charge, which is, in some sense, an indication of the quality of the fit. Note that the α-carbon partial charge is nearly constant in all three electronic states whereas the partial charges on carbons 2 and 3 change by more than a factor of three between the ground and excited states.

2. Benzyl Radical$(Ar)_1$

Figure 4 shows the MRES of the benzyl radical$(Ar)_1$ cluster. Transition energies and spectral shifts for this cluster relative to the bare benzyl radical are listed in Table IV. Spectral shifts for this cluster suggest that the feature labeled $6a_0^1$ is built on the 1^2A_2 origin and that features A_1 and A_2 are of a different nature. In addition, the van der Waals vibrational structure following A_1 and A_2, which is much less intense for the $1^2A_2\ 0_0^0$ and $6a_0^1$ features, also supports this assignment. As discussed above, A_1 and A_2 arise from vibronic interaction between the 1^2A_2 and 2^2B_2 electronic states,[19] consistent with these observations.

Note also that the benzyl radical$(Ar)_1$ spectrum terminates at ca. 450 cm^{-1} above the 1^2A_2 origin as can be seen by the presence of the $6a_0^1$ feature but not of A_3. If intracluster energy redistribution (IVR) and vibrational predissociation (VP) of the cluster are fast on the time scale of our experiment (roughly 10 ns), this intensity pattern suggests that the binding energy for benzyl radical$(Ar)_1$ is greater than 440 cm^{-1} and less than 650 cm^{-1}. Furthermore, the 1^2A_2 and 2^2B_2 states must be significantly coupled. If this latter electronic state mixing did not exist, a vibronic cluster spectrum built on the $2^2B_2\ 0_0^0$ state would extend for another ca. 450 cm^{-1} to the blue. This spectrum is not observed.

Exponential-6 potential energy calculations are performed for the benzyl radical$(Ar)_1$ cluster based on the potential energy function of eq.(1) and the parameters given in Table I for the D_0 1^2B_2 state. The results are presented in Table V. In order to learn more about the interaction between the benzyl radical and the various solvents, we attempt to model the excited state radical/solvent interaction to predict spectroscopic shifts and eventually cluster van der Waals modes. The benzyl radical excited states are fit to this potential form by artificially adjusting the carbon van der Waals parameters of the benzyl radical so as to reproduce the benzyl radical$(Ar)_1$ spectroscopic shifts (see Table IV; this assumes binding energy is directly related to transition energy of the chromophore). Specifically, the carbon-carbon interaction well-depth for the 1^2A_2 electronic state, which is proportional to the constants A and C of eq. (1), is increased by 15.3%,

and the well depth for the 2^2B_2 electronic state is increased by 8.5%. This artificial adjustment of the carbon van der Waals parameters has little, if any, physical justification; nonetheless, it proves to be instructive to examine if these simple changes in parameters for the benzyl radical can roughly account for the observed spectroscopic shifts, binding energies, and van der Waals vibrational/torsional modes of the remaining cluster systems.

Excited state binding energy for the argon cluster, as listed in Table V, is ca. 420 cm^{-1}. This value appears to be somewhat low, since it is outside the bracketed region of 440-650 cm^{-1}. If, however, dynamics of the cluster are not sufficiently rapid on the time scale of our experiment, then intensity contained in the $6a_0^1$ feature will lead to an overestimated lower limit for binding energy, consistent with the experimental results. Such dynamical factors have been observed for the benzene$(Ar)_1$ cluster.[45]

Figure 5 shows the benzyl radical$(Ar)_1$ cluster structure. The argon atom is calculated to lie directly above the aromatic ring system and slightly toward the α-carbon moiety. This structure is similar to that of the benzene$(Ar)_1$ cluster.[45]

A further test of our empirical model is to account for the van der Waals vibrations present in the benzyl radical$(Ar)_1$ cluster spectrum. Table VI tabulates the results of such calculations. The three van der Waals cluster modes are determined in the harmonic limit by numerically mapping out the one-dimensional potential energy functions, fitting the potentials to a quadratic function, and calculating the reduced mass from the benzyl radical and argon entities. In the notation of Table VI, the plane of the benzyl radical is the xy-plane with the y-axis being the principle axis of the benzyl radical. A vibration of the argon atom against the aromatic ring plane (z-axis motion) is seen to yield the largest vibrational energy mode at ca. 43 cm^{-1}, with x- and y-translational motion parallel to the aromatic ring plane results in vibrations at 11 and 10 cm^{-1}, respectively. The bottom portion of Table VI assigns the observed vibrations. Reasonable overall agreement exists between the calculated and observed van der Waals modes.

3. Benzyl Radical$(N_2)_1$

The MRES of the benzyl radical$(N_2)_1$ cluster is presented in Figure 6. It is similar to that of the benzyl radical$(Ar)_1$ spectrum with a few important and interesting differences: the relative intensities for the A_2 and $6a_0^1$ transitions are smaller than for the bare benzyl radical and benzyl radical$(Ar)_1$ cluster; the observed spectroscopic shifts (see Table IV) are smaller than for the benzyl radical$(Ar)_1$ cluster; intense van der Waals mode structure is observed at the $1^2A_2 \leftarrow 1^2B_2$ origin and at the A_1 vibronic feature; and this van der Waals mode structure is different for the 1^2A_2 and A_1 transitions. We will discuss each of these observations in turn below.

The decrease in intensity of the A_2 and $6a_0^1$ features relative to the $1^2A_2\ 0_0^0$ and A_1 features may suggest that the cluster undergoes dissociation at ca. 400 cm^{-1} above the $1^2A_2\ 0^0$ state. One would not expect that such an intensity decrease would result from changes in Franck-Condon factors for these two transitions, considering the results for the other clusters discussed in this report. The calculated binding energies for the benzyl radical$(N_2)_1$ cluster are given in Table V. Since the calculated binding energy for the cluster is ca. 530 cm^{-1}, the potential energy function used apparently overestimates the binding energy by roughly 100 cm^{-1}.

Table V lists derived spectroscopic shifts for the benzyl radical$(N_2)_1$ cluster system. The calculated shift for the $1^2A_2\ 0_0^0$ origin feature of -32.4 cm^{-1} is a factor of two larger than the observed shift of -16.6 cm^{-1} (Table IV), and the shift for A_2 of -5.78 cm^{-1} is also larger than the observed shift of -0.7 cm^{-1} (Table IV). The calculations do correctly predict the trend, however, yielding a smaller shift for the vibronically mixed states. Table V shows that the electrostatic part of the intermolecular potential for this cluster is important, contributing a total of 20% to the binding energy, as is to be expected for N_2 because of its large quadruple moment.[44]

The calculated 1^2B_2 benzyl radical$(N_2)_1$ cluster structure is shown in Figure 7. The nitrogen molecule is calculated to lie above the plane of the benzyl radical with its bond axis parallel to the benzyl radical x-axis (see Table III). Calculation of the structure of the benzyl radical$(N_2)_1$ cluster in the 1^2A_2 electronic state shows the same general structure as the ground state cluster except that the nitrogen molecule is displaced by 0.07 Å along the positive y-axis (see Table III).

A similar calculation for the cluster structure in the 2^2B_2 electronic states yield a geometry in which the nitrogen molecule bond axis is parallel to the benzyl radical y-axis (see Table III and Figure 7). These calculated results are qualitatively consistent with the observed van der Waals vibrational mode structure built on the 1^2A_2 0_0^0 and A_1 features of Figure 6: the spectroscopic structure observed for the 1^2A_2 origin corresponds to a vibrational van der Waals mode progression and the structure at A_1 is reminiscent of internal rotation such as that observed and assigned for the benzene$(N_2)_1$ cluster.[46] The rotor transitions observed here may also be associated with relatively free rotation of the N_2 molecule above the plane of the benzyl radical as we now discuss.

A quantitative interpretation of the spectroscopic structure at the 1^2A_2 electronic origin and A_1 features of Figure 6 can, in principle, be accomplished through the use of empirical potential calculations. The solid lines in Figure 8 show the potential energy functions generated by translating the N_2 molecule along the ± y-axis relative to its calculated minimum energy location. The small displacement between the minima of the $D_0(1^2B_2)$ and $D_1(1^2A_2)$ potentials of 0.07 Å is barely noticeable. The dashed lines correspond to the two quadratic potentials which best fit the two exponential-6-Coulomb atom-atom potentials (Eq. (1)) near their minima. The calculated potential curves are generated by optimizing all but the one degree of freedom of interest. The fitted functions used are of the form $V=(1/2)k\,\Delta y^2$, in which k for both the 1^2B_2 and 1^2A_2 states is coincidentally found to be 100 $cm^{-1}/Å^2$. The harmonic vibrational levels using this value for k and the reduced mass for this translational motion [i.e., $M_{BR}M_{N2}/(M_{BR} + M_{N2})$] are shown in Figure 8. These derived (harmonic) potentials are employed to calculate the Franck-Condon intensities displayed in Figure 6. The calculated vibrational spacing of 12.5 cm^{-1} is a factor of two lower than the observed value of 25.0 cm^{-1}, but the relative transition intensities are close to those observed.

A similar calculation can be performed for the van der Waals structure built on the A_1 feature (2^2B_2 mixed vibronic state) shown in Figure 6. Due to the rotational displacement of the N_2 molecule in the 2^2B_2 electronic state with respect the ground 1^2B_2 state, a potential energy

function corresponding to rotation of the N_2 molecule is generated. The solid lines in Figure 9 show the rotational potential energy function obtained for N_2 rotation in the 1^2B_2 and 2^2B_2 electronic states. A two-fold potential is seen to exist with barriers of 13.0 and 17.2 cm^{-1}, respectively. The molecular symmetry group which characterizes this two-fold potential is the G_2 group. The G_2 group is isomorphic to the C_s molecular point group: details of the generation of this molecular symmetry group as well as the labeling of the rotor levels are given elsewhere.[47,48] The dashed line in Figure 9 is the 2^2B_2 potential which best reproduces the observed transitions. Table VII lists the observed and calculated transitions within this potential model. The agreement is remarkable, if not fortuitous, between the experimental and calculated potential functions.

4. Benzyl Radical$(CH_4)_1$

The benzyl radical$(CH_4)_1$ cluster spectrum is presented in Figure 10. The intensity of the $1^2A_2\ 0_0^0$ and $6a_0^1$ features of Figure 10 compared to those of the bare radical (Figure 3), as well as the complete lack of higher energy features such as A_3, suggests the cluster binding energy lies between 440 and 650 cm^{-1}. The calculated binding energy from Table V of ca. 540 cm^{-1} for this cluster is consistent with the experimental results.

The observed spectral shifts for the benzyl radical$(CH_4)_1$ cluster are listed in Table IV: they are roughly twice those observed for the argon cluster, and three times those of the nitrogen cluster. The calculated shifts given in Table V agree well with the experimentally observed values. The vibronically mixed states have smaller shifts than the pure 1^2A_2 states and are of the correct magnitude.

The 1^2A_2, A_1, A_2, and $6a_0^1$ features of Figure 10 all contain rich spectroscopic structure associated with low energy van der Waals motion. The type of motion giving rise to such structure is likely a combination of methane rotation and vibration, such as that observed for the benzene$(CH_4)_1$ cluster. Empirical potential energy calculations for benzene$(CH_4)_1$ show that methane is situated on the aromatic ring system with three hydrogens positioned toward carbon-carbon bonds giving rise to a cluster of effective C_{3v} symmetry.[49] Calculated low energy van der

Waals motion for this cluster consists of methane rotation described by a three-fold potential energy function plus cluster vibrational motion. Methane contains both three-fold and two-fold rotational axes. Insight into the preferred type of rotor motion may be obtained from calculated cluster equilibrium structures in the various electronic states. Figure 11 shows these calculated structures. Both the 1^2B_2 and 1^2A_2 electronic states have similar asymmetric (double-well) structures with methane located near the α-carbon moiety. The calculated methane configuration for these two electronic states is such that neither a pure "two hydrogen down" nor "three hydrogen down" structure exists. Internal rotational motion of the methane molecule will most likely occur but the axis of its rotation is uncertain. The double-well potentials for methane in the benzyl radical 1^2B_2 and 1^2A_2 states may greatly effect the observed spectra. For the 2^2B_2 electronic state a symmetric (single-well) "three hydrogen down" methane structure is calculated. The expected internal rotational motion for this latter state would be one arising from a three-fold potential energy term.

Table VIIIa lists the observed spectroscopic features for the 1^2A_2 0_0^0 and $6a_0^1$ regions with assignments based on either a three-fold (G_3 molecular symmetry group) or two-fold (G_2 molecular symmetry group) potential energy function. The top portion of Table VIIIa presents results for the benzyl radical$(CH_4)_1$ cluster spectrum of Figure 10 and the bottom portion of the Table VIIIa lists results for deuterated methane. Examining first the G_3 assignments, four out of six observed features can be assigned as methane rotational transitions; the remaining two features, by default, are assigned as cluster vibrational modes. Credibility to the 15.0 and 13.5 cm^{-1} assignments is obtained by calculating the reduced mass isotope correction factor, $[\mu_H/\mu_D]^{1/2} = 0.91$, which correctly predicts the isotopic shift for a cluster vibrational mode treated as an uncoupled harmonic oscillator. In a similar fashion, the G_2 assignment of the same features can account for all but one of the observed features as arising from methane rotation. Both the G_3 and G_2 assignments contain only the barrier height as an adjustable parameter. Unfortunately, the rotational constant for methane is identical for both three-fold and two-fold rotor motion.

A similar ambiguity in feature assignment arises for motion accompanying the A_1 and A_2 features of Figure 10. Table VIIIb lists the observed features and assignments. Ironically, the same barrier height employed in the calculations presented in Table VIIIa fits the spectroscopic data listed in Table VIIIb. Fewer features are observed for these vibronically mixed states, nonetheless the same situation arises: both G_3 and G_2 assignments can be made of the data.

The empirical potential energy calculations can be used in a straightforward way to extract barrier heights for three-fold and two-fold rotor motion. The calculations should be able to distinguish which type of motion is occurring. The lowest barriers found for three-fold rotational motion are 21.5, 32.6, and 136.5 cm^{-1} for the 1^2B_2, 1^2A_2, and 2^2B_2 electronic states, respectively. Two-fold barriers in excess of 200 cm^{-1} are obtained for the same three electronic states. The calculations are, therefore, unable to predict accurate barrier heights for the rotor motion. Two important results can be extracted from the above discussion. First, the calculations succeed in predicting the benzyl radical$(N_2)_1$ rotational barrier is not repeated for the methane cluster system. Second, and equally important, care must be exercised in extracting a rotational barrier from spectroscopic data which include low energy van der Waals vibrational modes.

5. Benzyl Radical$(C_2H_6)_1$

The benzyl radical$(C_2H_6)_1$ cluster spectrum is presented in Figure 12. The A_1 feature is seen to be much more intense than the remaining features. In addition, the presence of the A_3 feature suggests a binding energy greater than 650 cm^{-1} exists for this cluster. This is consistent with the calculated binding energies listed in Table V. Two stable conformations are calculated and are pictorially represented in Figure 13. The more stable of the two conformers of this cluster, labeled **1**, has ethane's carbon-carbon bond axis nearly parallel to the benzyl radical principle axis. Structure **2** has the ethane carbon-carbon bond nearly parallel to the benzyl radical x-axis (see Table III). In Figure 12 we have assigned the well-resolved spectroscopic structure to the lowest energy conformer **1**. The broad feature in the vicinity of the A_1, A_2, and $6a_0^1$ transitions be may

due to van der Waals vibrational structure or the presence of transitions associated with the cluster structures labeled **2**.

The spectroscopic shifts corresponding to conformation **1** are listed in Table IV. The corresponding calculated shifts in Table V overestimate the observed shifts by roughly 10 cm^{-1} for the 1^2A_2 states, and 20 cm^{-1} for the vibronically mixed states.

Low energy van der Waals modes are observed for this cluster species as in the cluster systems already discussed. Due to the increased complexity of the spectrum and possible existence of multiple conformations, an analysis of the vibrational van der Waals modes is not attempted.

6. Benzyl radical$(C_3H_8)_1$

The benzyl radical$(C_3H_8)_1$ cluster spectrum is presented in Figure 14. It is similar to that found for the ethane cluster spectrum of (Figure 12) in that the A_1 feature has the largest intensity and the A_3 feature is observed. Additional spectroscopic structure to the blue of the A_3 feature up to roughly 1000 cm^{-1} is consistent with the calculated binding energy of ca. 970 cm^{-1} listed in Table V. No features are observed to the blue of the spectrum shown. Three stable structural conformations are calculated for this cluster, with ground state binding energies given in Table V and pictorial representations shown in Figure 15. The lowest energy structure, **1**, has propane's three carbon atoms lying in the yz plane perpendicular to the xy plane of the benzyl radical (see Table III); structure **2** has propane's three carbon atoms lying in a plane parallel to the plane of the benzyl radical (xy) above carbons 2, 3, 4, and 5 of the benzyl radical (see Table III); and structure **3** has propane's three carbon atoms also in a plane parallel to that of the benzyl radical xy plane above carbons 2 and 3 (see Table III). Similar results have been found for the toluene/propane cluster system.[50] A structural conformation assignment of the features in Figure 14 is not unique. A plausible scheme can label the most intense features (1^2A_2, A_1, A_2, 6a, and A_3) as belonging to structure **1**, and the weaker, red-shifted, features to a second conformation such as **2** (or **3**). Such difficulties in conformation assignment also make van der Waals mode assignment prohibitively complex.

V. CONCLUSIONS

In this report we have presented spectra and calculations for the benzyl radical solvated with the non-polar solvents Ar, N_2, CH_4, C_2H_6, and C_3H_8. The experimentally observed solvation effects of the benzyl radical are not dissimilar from those found for the benzene system:[45,46,49] small spectral red shifts, the presence of van der Waals modes, and binding energies in the range of 400 to 950 cm^{-1}.

The varied solvents studied here allow a test of empirical atom-atom based potential energy calculations to be performed. Binding energies for the argon and nitrogen clusters are overestimated by roughly 50-100 cm^{-1}, whereas for the hydrocarbon solvents the calculated binding energies are consistent with the experimental results. The predicted trends of the spectroscopic shifts for all the solvents examined are accurately modeled, but the size of the shifts are incorrect by as much as a factor of three. The calculated van der Waals low energy vibrational/torsional modes yield mixed results: for argon and nitrogen the calculations are of predictive value while for methane the derived internal rotational barriers are too large. Certainly there is room for improvement as far as atom based van der Waals parameters are concerned. An interesting area to explore theoretically is the possibility of ab initio derived atom-based van der Waals parameters. If such a theoretical advance is made, better modeling of excited states (without assumptions about atomic van der Waals parameters) would become tractable.

REFERENCES

1. B. Meyer, **Low Temperature Spectroscopy** (Elsevier, N. Y., 1971).
2. M. J.Almond and A. J.Downs, **Spectroscopy of Matrix Isolated Species**, (Wiley, N. Y., 1989).
3. S. Cradock and A. J. Hinchcliffe, **Matrix Isolation**, (Cambridge, N. Y., 1975).
4. L. Andrews and M. Moskovits, **Chemistry and Physics of Matrix Isolated Species**, (Elsevier, N. Y., 1989).
5. W. T. Borden, **Diradicals**, (Wiley, N. Y., 1982).
6. S. C. Foster and T. A. Miller, J. Phys. Chem. **93**, 5986 (1989).
7. M. E. Jacox, J. Phys. Chem. Ref. Data **13**, 945 (1984).
8. M. E. Jacox, J. Phys. Chem. Ref. Data **17**, 269 (1988).
9. H.-S. Im and E. R. Bernstein, J. Chem. Phys. **95**, 6326 (1991).
10. M. Fukushima and K. Obi, J. Chem. Phys. **93**, 8488 (1990).
11. J. I. Selco and P. G. Carrick, J. Mol. Spect. **137**, 13 (1989).
12. M. Heaven, L. Dimauro and T. A. Miller, Chem. Phys. Lett. **95**, 347 (1983).
13. M. A. Hoffbauer and J. W. Hudgens, J. Phys. Chem. **89**, 5152 (1985).
14. T. Ebata, K. Obi and I. Tanaka, Chem. Phys. Lett. **77**, 480 (1981).
15. N. Ikeda, N. Nakashima and K. Yoshihara, J. Chem. Phys. **82**, 5285 (1985).
16. C. Cossart-Magos and W. Goetz, J. Mol. Spect. **115**, 366 (1986).
17. D. M. Friedrich and A. C. Albrecht, J. Chem. Phys. **58**, 4766 (1973).
18. C. Cossart-Magos and S. Leach, J. Chem. Phys. **56**, 1534 (1972).
19. C. Cossart-Magos and S. Leach, J. Chem. Phys. **64**, 4006 (1976).
20. G. Porter and E. Strachan, Spectrochimica Acta **12**, 299 (1958).
21. G. Porter and F. J. Wright, Trans. Faraday Soc. **51**, 1469 (1955).
22. G. Porter and I. Norman, Proc. Roy. Soc. A **230**, 399 (1953).
23. G. Porter and M. W. Windsor, Nature (Lond.) **180**, 187 (1957).
24. J. E. Rice, N. C. Handy, P. J. Knowles, J. Chem. Soc. Far. Trans., **83**, 1643 (1987).

25. F. Negri, G. Orlandi, F. Zerbetto, M. Z. Zgierski, JCP, **93**, 600 (1990).

26. G. Orlandi, G. Poggi, F. Zerbetto, Chem. Phys. Lett., **115**, 253 (1985).

27. H. M. Chang and H. H. Jaffe, Chem. Phys. Lett. **23**, 341 (1974).

28. N. Kanamaru and S. Nagakura, Bull. Chem. Soc. Jpn. **43**, 3443 (1970).

29. J. Wasilewski, Acta Phys. Pol. A **46**, 341 (1974).

30. J. C. Shug and D. H.Phillips, J. Chem. Phys. **49**, 3734 (1968).

31. W. Bingel, Z. Naturf. **10A**, 462 (1955).

32. H. C. Longuett-Higgins and J. A. Pople, Proc. Phys. Soc. Lond. **68A**, 591 (1955).

33. N. S. Isaacs, **Reactive Intermediates in Organic Chemistry**, (Wiley, N.Y., 1974), and references therein.

34. E. R. Bernstein, K. Law and M. Schauer, J. Chem. Phys. **80**, 207 (1984).

35. M. Dupuis, A. Farazdel, **HONDO**, (IBM Corp., Center for Scientific & Engineering Computations, Kingston, N.Y., 1990).

36. S. R. Cox and D. E. Williams, J. Comp. Chem. **2**, 304 (1981).

37. L. E. Chirlian and M. M. Francl, J. Comp. Chem. **6**, 894 (1987).

38. J. D. Westbrook, R. M. Levy, and K. Krogh-Jespersen, J. Comp. Chem., in press.

39. S. L. Mayo, B. D. Olafson, W. A. Goddard, J. Phys. Chem. **94**, 8897 (1990).

40. N. Karasawa, S. Dasgupta, W. A. Goddard, J. Phys. Chem. **95**, 2260 (1991).

41. W. H. Press, B. P. Flannery, S. A. Teukolsky, W. T. Vetterling, **Numerical Recipes: The Art of Scientific Computing**, (Cambridge, N. Y., 1989).

42. G. Herzberg **Molecular Spectra and Molecular Structure II. Infrared and Raman Spectra of Polyatomic Molecules**, (van Nostrand Reinhold Co., 1945).

43. D. E. Williams and S. R. Cox, Acta Crystallogr. Sect. B **40**, 404 (1984).

44. F. P. Billingsley and M. Krauss, J. Chem. Phys. **60**, 2767 (1974).

45. T. A. Stephenson, S. A. Rice, J. Chem. Phys. **81**, 1083 (1984).

46. R. Nowak, J. A. Menapace, E. R. Bernstein, J. Chem. Phys. **89**, 1309 (1988).

47. H. C. Longuett-Higgins, Mol. Phys. **6**, 445 (1963).

48. P. R. Bunker, **Molecular Symmetry and Spectroscopy**, (Academic, N.Y., 1979).

49. J. A. Menapace, E. R. Bernstein, J. Phys. Chem. **91**, 2843 (1987).

50. M. Schauer, K. Law, E. R. Bernstein, J. Chem. Phys. **82**, 726, 736 (1985).

51. J. O. Hirschfelder, C. F. Curtis, R. B. Bird, **Molecular Theory of Gases and Liquids**, (Wiley, N. Y., 1954).

Table I. Non-bonded Interaction Parameters for the D_0 (1^2B_2), D_1 (1^2A_2), and D_2 (2^2B_2) Electronic States.

Species	A (kcal/mol)	B ($Å^{-1}$)	C ($Å^6$ kcal/mol)
Benzyl Radical D_0 / Solvent Parmeters:			
Carbon[a]	30026.	3.3845	472.2
Hydrogen[a]	1687.6	3.537	43.42
Nitrogen[b]	60862.	3.7801	329.5
Argon[c]	40103.	3.1258	1577.
Benzyl Radical D_1 Parameters:[d]			
C	34620.	3.3845	544.5
H	1687.6	3.537	43.42
Benzyl Radical D_2 Parameters:[d]			
C	32578.	3.3845	512.3
H	1687.6	3.537	43.42

[a] Ref. 40.

[b] Ref. 43.

[c] Ref. 51.

[d] These parameters are obtained by adjusting the carbon parameters so as to reproduce the experimentally measured benzyl radical$(Ar)_1$ spectroscopic shifts. See text and Tables IV and V.

Table II. Ab Initio Calculations of the Excited States of the Benzyl Radical.

Transition Energy Estimation:

State Symmetry	Root[a]	Energy (a.u.) RHF optimized geometry[b]	Energy (a.u.) CASSCF optimized geometry[b]
B_2	first	-269.128883 (0.0)	-269.128961 (0.0)
B_2	second	-269.017838 (2437 cm^{-1})	-269.024851 (22852 cm^{-1})
A_2	first	-269.012503 (25545 cm^{-1})	-269.021319 (23627 cm^{-1})

[a] Active space consists of 7 π orbitals (Dunning-Huzinaga [9s,5p] double zeta valence basis set). RHF result: $(b_2)^2\ (b_2)^2\ (a_2)^2\ (b_2)^1\ (a_2)\ (b_2)\ (b_2)$, B_2 state symmetries resulted in 404 configurations, and A_2 state symmetries resulted in 380 configurations.

[b] Energy gradients reduced to less than 10^{-4} hartree/bohr.

Ionization Energy Estimation:

UHF B_2 ground state energy = -269.071160

RHF A_1 + 1 cation energy = -268.801410

Calculated I.P. = 59,210 cm^{-1}, observed I.P. = 58,358 cm^{-1} (See Ref. 9).

Table III. Calculated Partial Charges for the Benzyl Radical in the 1^2B_2, 1^2A_2, and 2^2B_2 Electronic States.[a] The number of grid points used for each electronic state is 519.

Benzyl Radical Axis System[b] and Numbering Scheme:

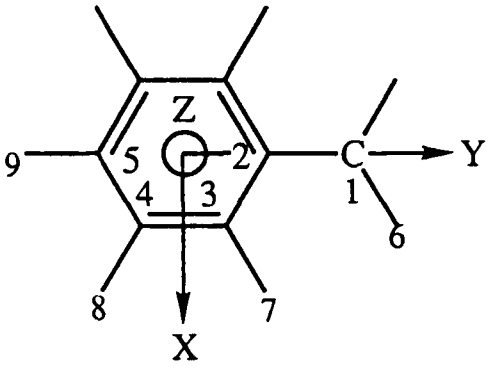

Electronic State	Atom	Partial Charge (e⁻)	Calc. Residual Charge (e⁻)
1^2B_2 (D_0)	1	-0.553	0.000410
	2	0.243	
	3	-0.149	
	4	-0.222	
	5	-0.104	
	6	0.203	
	7	0.139	
	8	0.163	
	9	0.144	
1^2A_2 (D_1)	1	-0.547	0.000917
	2	0.063	
	3	-0.023	
	4	-0.184	
	5	-0.167	
	6	0.207	
	7	0.107	
	8	0.144	
	9	0.150	
2^2B_2 (D_2)	1	-0.654	0.000744
	2	0.540	
	3	-0.350	
	4	-0.164	
	5	-0.041	
	6	0.214	
	7	0.175	
	8	0.150	
	9	0.105	

[a] CASSCF 1^2B_2 optimized geometry used, grid spacing = 2.0 bohr, and shell thickness = 4.0 bohr.

[b] The origin of the axis system corresponds to the center-of-mass of the benzyl radical.

Table IV. Observed Spectroscopic Transitions and Shifts of the Benzyl Radical and Its Clusters.

Species	Excited State Feature (cm^{-1})					Relative Shift (cm^{-1})		
	Origin	A_1	A_2	$6a_0^1$	$1^2A_2 0_0^0$	A_1	A_2	$6a_0^1$
Benzyl Radical	21995.6	22323.2	22383.7	22428.8	-	-	-	-
Benzyl Radical$(Ar)_1$	21971.7	22309.6	22369.0	22407.6	-23.9	-13.6	-14.7	-21.2
Benzyl Radical$(N_2)_1$	21979.0	22322.5	22380.0	22415.6	-16.6	-0.7	-3.7	-13.2
Benzyl Radical$(CH_4)_1$	21953.7	22294.0	22352.3	22389.8	-41.9	-29.2	-31.4	-39.0
Benzyl Radical$(C_2H_6)_1$	21962.9	22304.1	22362.8	22399.3	-32.9	-19.1	-20.9	-29.5
Benzyl Radical$(C_3H_8)_1$ [a]	21965.8	22301.0	22363.9	22401.8	-29.8	-22.2	-19.8	-27.0

[a] Multiple conformations are believed to exist for the propane cluster. The listed values correspond to the most intense transitions.

Table V. Calculated Binding Energies (V_{BE} cm^{-1}) for Benzyl Radical Clusters in Different Electronic States and Derived Spectroscopic Shifts for the Two Observed Transitions.

	V_{BE}	= V_{VDW}	+ V_C	Cluster Shift, ΔE
1^2B_2:				
Ar	-399.5	-399.5	0	
N_2	-519.5	-422.7	-96.8	
CH_4	-509.2	-493.3	-15.9	
C_2H_6 (1)	-708.7	-707.9	-0.8	
C_2H_6 (2)	-666.6	-685.6	19.0	
C_3H_8 (1)	-930.0	-898.8	-31.2	
C_3H_8 (2)	-865.1	-852.1	-13.0	
C_3H_8 (3)	-855.2	-879.7	24.5	
1^2A_2:[a]				
Ar	-423.3	-423.3	0	-23.8
N_2	-551.9	-447.9	-103.9	-32.4
CH_4	-544.3	-519.5	-24.8	-35.1
C_2H_6 [b]	-748.2	-753.3	5.1	-39.5
C_3H_8 [b]	-976.3	-957.1	-19.2	-46.3
2^2B_2:[a]				
Ar	-412.9	-412.9	0	-13.4
N_2	-525.2	-436.0	-89.2	-5.7
CH_4	-534.3	-540.7	6.4	-25.1
C_2H_6 [b]	-751.1	-723.4	-27.7	-42.4
C_3H_8 [b]	-971.2	-920.4	-50.8	-41.2

[a] The binding energies for the excited states are calculated by adjusting the 1^2A_2 and 2^2B_2 carbon parameters to reproduce spectroscopic shifts for benzyl radical$(Ar)_1$. The calculated shifts for the remaining clusters are obtained using the modified excited state van der Waals parameters and appropriate partial charges for each electronic state (see Table I).

[b] Only lowest energy conformer result is presented here.

Table VI. Benzyl Radical$(Ar)_1$ Calculated van der Waals Vibrations and Assignments.

Mode Calculation:

Electronic State	mode (cm^{-1}) t_x	t_y	t_z
1^2B_2	11.0	10.1	43.4
1^2A_2	11.4	10.4	43.9
2^2B_2	11.2	10.4	43.4

vdW Mode Assignment:

	Observed	Calculated[b]	
1^2A_2	41.2	t_z	43.9
A_1	6.9	t_y	10.4
	22.4	$t_x t_y$	21.8
	38.9	t_y^4	41.6
	43.4	t_z	43.4
A_2	6.0	t_y	10.4
	14.5	t_x	11.2
$6a^1$	13.0	t_x	11.4
	40.2	t_z	43.9

[a] Plane of aromatic ring is the xy-plane, the y-axis is the principle axis (see Table III).
[b] Calculated modes for the 1^2A_2 and $6a^1$ states are obtained using 1^2A_2 state van der Waals parameters, whereas A_1 and A_2 state modes are obtained using 2^2B_2 state van der Waals parameters.

Table VII. Benzyl Radical$(N_2)_1$ Internal Rotational Transitions.

Observed Transitions[a]	Assignment	Calculated Transitions[b]
0.0	0a' ← 0a'	0.0
1.0	1a'' ← 0a'	0.2
6.0	2a' ← 0a'	8.6
11.0	3a'' ← 0a'	10.8
15.0	4a' ← 0a'	14.4
17.0	vdw vib.	- -
22.0	5a'' ← 0a'	22.0
24.0	6a' ← 0a'	22.6

[a] Transitions are relative to the A_1 feature located at 22,322.5 cm^{-1}.

[b] The potential function is $V=V_2/2(1-\cos 2\phi)$ with $V_2=18.0\ cm^{-1}$, $B=2.0\ cm^{-1}$.

Table VIIIa. Benzyl Radical(methane)$_1$ Low Energy Modes for the 1^2A_2 0_0^0 and $6a_0^1$ Transitions.

Benzyl Radical$(CH_4)_1$

Observed (cm^{-1})[a]	G_3 assignment[b]	Calc.	G_2 assignment[c]	Calc.
0.0	0a ← 0a	0.0	0a' ← 0a'	0.0
4.8	1e ← 1e	5.2	1a" ← 0a'	4.7
15.0	vdw. vib.	-	2a' ← 1a"	15.1
19.8	2e ← 1e	20.9	2a' ← 0a'	20.8
38.7	vdw. vib.	-	3a" ← 1a"	41.8
45.9	3a ← 0a	46.8	3a" ← 0a'	46.8

Benzyl Radical$(CD_4)_1$

Observed (cm^{-1})[d]	G_3 assignment[b]	Calc.	G_2 assignment[c]	Calc.
0.0	0a ← 0a	0.0	0a' ← 0a'	0.0
5.0	1e ← 1e	2.6	2a' ← 1a"	7.3
9.9	2e ← 1e	10.5	2a' ← 0a'	10.5
13.5	vdw. vib .	-	vdw. vib.	-
20.1	3a ← 0a	23.4	3a" ← 1a"	20.4
24.3	vdw. vib.	-	3a" ← 0a'	23.5

[a] Relative to 1^2A_2 electronic origin located at 21953.7 cm^{-1}.

[b] Calculated using $V_3/2(1-\cos 3\phi)$ potential with V_3=3.0 cm^{-1} and B=5.2 cm^{-1} for CH_4 or B=2.6 cm^{-1} for CD_4.

[c] Calculated using $V_2/2(1-\cos 2\phi)$ potential with V_2=2.0 cm^{-1} and B=5.2 cm^{-1} for CH_4 or B=2.6 cm^{-1} for CD_4.

[d] Relative to 1^2A_2 electronic origin located at 21954.5 cm^{-1}.

Table VIIIb. Benzyl Radical(methane)$_1$ Low Energy Modes for the A_1 and A_2 Electronic Transitions.

Benzyl Radical(CH_4)$_1$

Observed (cm^{-1})[a]	G_3 assignment[b]	Calc.	G_2 assignment[c]	Calc.
0.0	0a ← 0a	0.0	0a' ← 0a'	0.0
4.0	1e ← 1e	5.2	1a" ← 0a'	4.7
13.9	vdw. vib.	-	2a' ← 1a"	15.1
18.9	2e ← 1e	20.9	2a' ← 0a'	20.8

Benzyl Radical(CD_4)$_1$

Observed (cm^{-1})[d]	G_3 assignment[b]	Calc.	G_2 assignment[c]	Calc.
0.0	0a ← 0a	0.0	0a' ← 0a'	0.0
4.0	1e ← 1e	2.6	2a' ← 1a"	7.3
9.1	2e ← 1e	10.5	2a' ← 0a'	10.5
20.1	3a ← 0a	23.4	3a" ← 1a"	20.4

[a] Relative to A_1 feature located at 22294.0 cm^{-1}.

[b] Calculated using $V_3/2(1-\cos 3\phi)$ potential with V_3=3.0 cm^{-1} and B=5.2 cm^{-1} for CH_4 or B=2.6 cm^{-1} for CD_4.

[c] Calculated using $V_2/2(1-\cos 2\phi)$ potential with V_2=2.0 cm^{-1} and B=5.2 cm^{-1} for CH_4 or B=2.6 cm^{-1} for CD_4.

[d] Relative to A_1 feature located at 22293.9 cm^{-1}.

FIGURE CAPTIONS

Figure 1. Optical arrangement for MRES study of radicals.

Figure 2. Electronics arrangement for MRES study of radicals.

Figure 3. The benzyl radical MRES. The features labeled A_1 and A_3 arise from vibronic coupling between the non-totally symmetric $6b^1$ vibration of the 1^2A_2 electronic state and the 2^2B_2 electronic origin. The feature labeled A_2 is assigned as the $18b^1$ vibration of the 1^2A_2 electronic state which vibronically couples and borrows intensity from the 2^2B_2 electronic origin. (See reference 19)

Figure 4. The benzyl radical$(Ar)_1$ spectrum. Note that the spectrum ends at roughly 450 cm^{-1} above the $1\ ^2A_2\ 0_0^0$ transition.

Figure 5. Calculated structure of the benzyl radical$(Ar)_1$ cluster in the $D_0\ 1^2B_2$ electronic state. The argon atom lies above the plane at z =3.50 Å and y = -.19 Å. The circle representing the argon atom corresponds to the argon van der Waals radius (~1.8 Å).

Figure 6. The benzyl radical$(N_2)_1$ spectrum. The calculated spectrum corresponds to a vibration of the N_2 molecule along the plane of the benzyl radical. See text for details of the calculation.

Figure 7. Calculated structure of the benzyl radical$(N_2)_1$ cluster in the $D_0\ 1^2B_2$ and $D_2\ 2^2B_2$ electronic states. The bond axis of the nitrogen molecule is parallel to the benzyl radical x-axis in D_0 and perpendicular to it in D_2 (see Table III).

Figure 8. The calculated potential energy surfaces corresponding to a van der Waals vibration of the N_2 molecule along the plane of the benzyl radical are shown for the D_0 and D_1 electronic states. Specifically, the one-dimensional functions represent the displacement, from its minimum energy location, of the N_2 entity along the y-axis shown in Table III.

Figure 9. The calculated potential energy surfaces corresponding to the N_2 rotation above the plane of the benzyl radical in the D_0 and D_2 electronic states (solid lines). The dashed line represents the fitted potential which best reproduces the spectroscopic data. See Table VII for the explicit form of the potential used.

Figure 10. The benzyl radical$(CH_4)_1$ MRES. Note that the spectrum ends at ca. 450 cm^{-1} above the $1\ ^2A_2\ 0_0^0$ transition.

Figure 11. Pictorial representation of the benzyl radical$(CH_4)_1$ cluster structure in the D_0, D_1, D_2 electronic states of the radical. Note the change in methane orientation between the $1\ ^2B_2$ and $1\ ^2A_2$ states, and the $2\ ^2B_2$ state.

Figure 12. The benzyl radical$(C_2H_6)_1$ MRES. Note that the spectrum ends at ca. 650 cm^{-1} above the $1\ ^2A_2\ 0_0^0$ transition.

Figure 13. Two structures for the benzyl radical$(C_2H_6)_1$ in the D_0 electronic state. The C–C bond axis of the ethane is nearly parallel to the y- or x-axis of the benzyl radical for Structures **1** and **2**, respectively.

Figure 14. The benzyl radical$(C_3H_8)_1$ MRES . Note that the spectrum extends beyond 900 cm^{-1} above the $1\ ^2A_2\ 0_0^0$ transition.

Figure 15. Three structures for the benzyl$(C_3H_8)_1$ cluster in the D_0 electronic state.

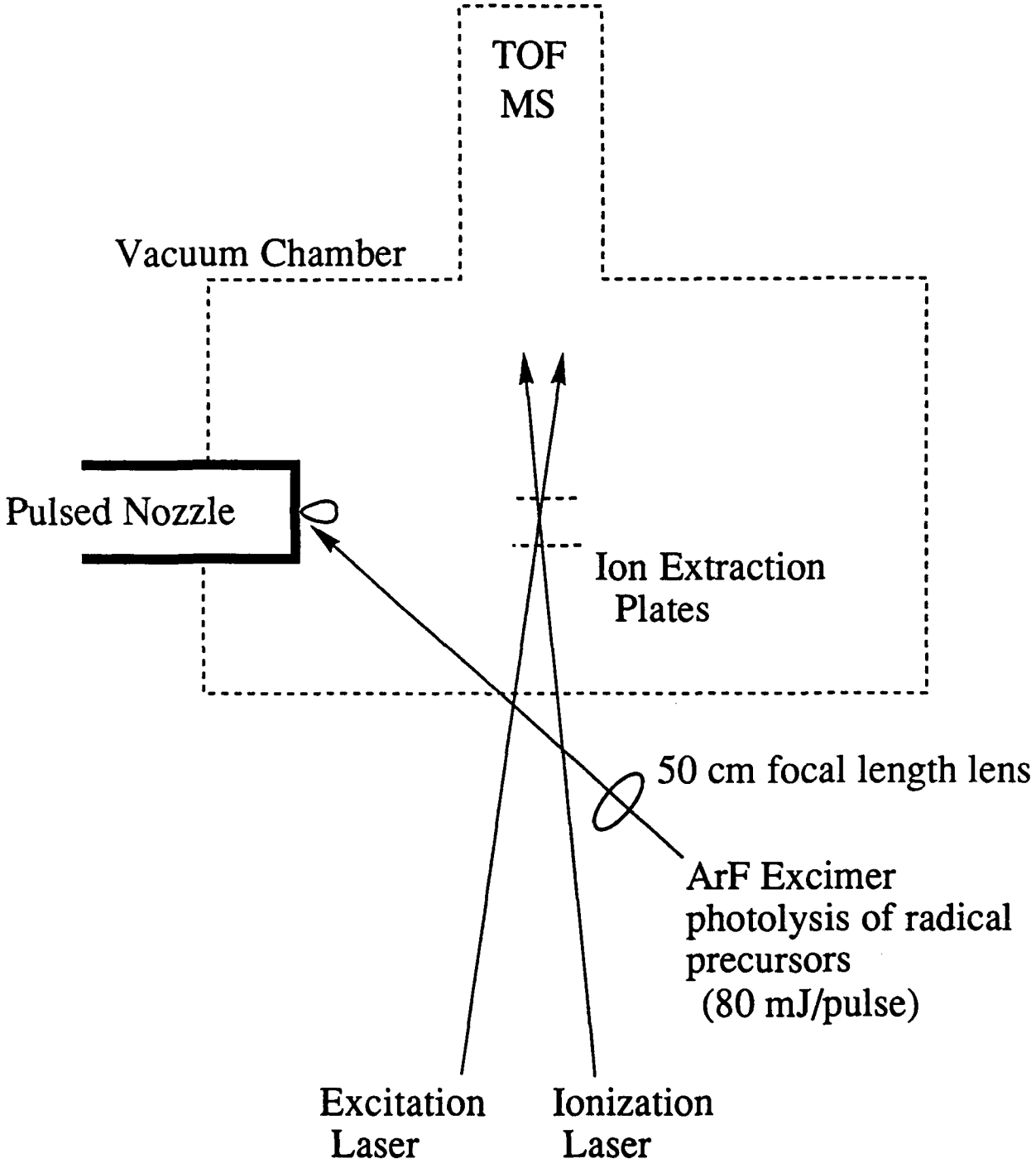
TOF
MS
Vacuum Chamber
Pulsed Nozzle
Ion Extraction
Plates
50 cm focal length lens
ArF Excimer
photolysis of radical
precursors
(80 mJ/pulse)
Excitation
Laser
Ionization
Laser

Figure 1

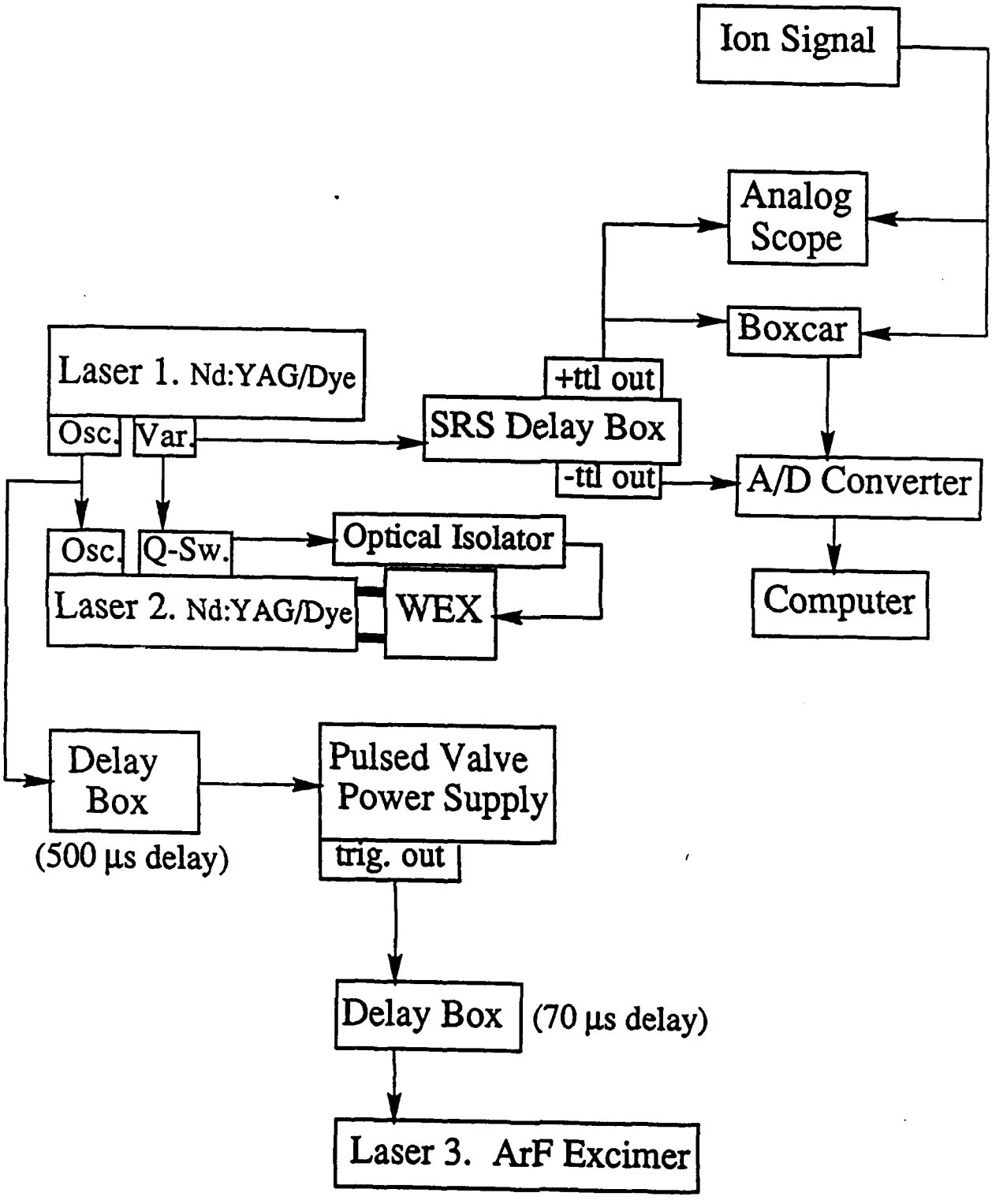
Ion Signal
Analog Scope
Boxcar
Laser 1. Nd:YAG/Dye
Osc.
Var.
+ttl out
SRS Delay Box
-ttl out
A/D Converter
Osc.
Q-Sw.
Optical Isolator
Laser 2. Nd:YAG/Dye
WEX
Computer
Delay Box
(500 µs delay)
Pulsed Valve Power Supply
trig. out
Delay Box
(70 µs delay)
Laser 3. ArF Excimer

Figure 2

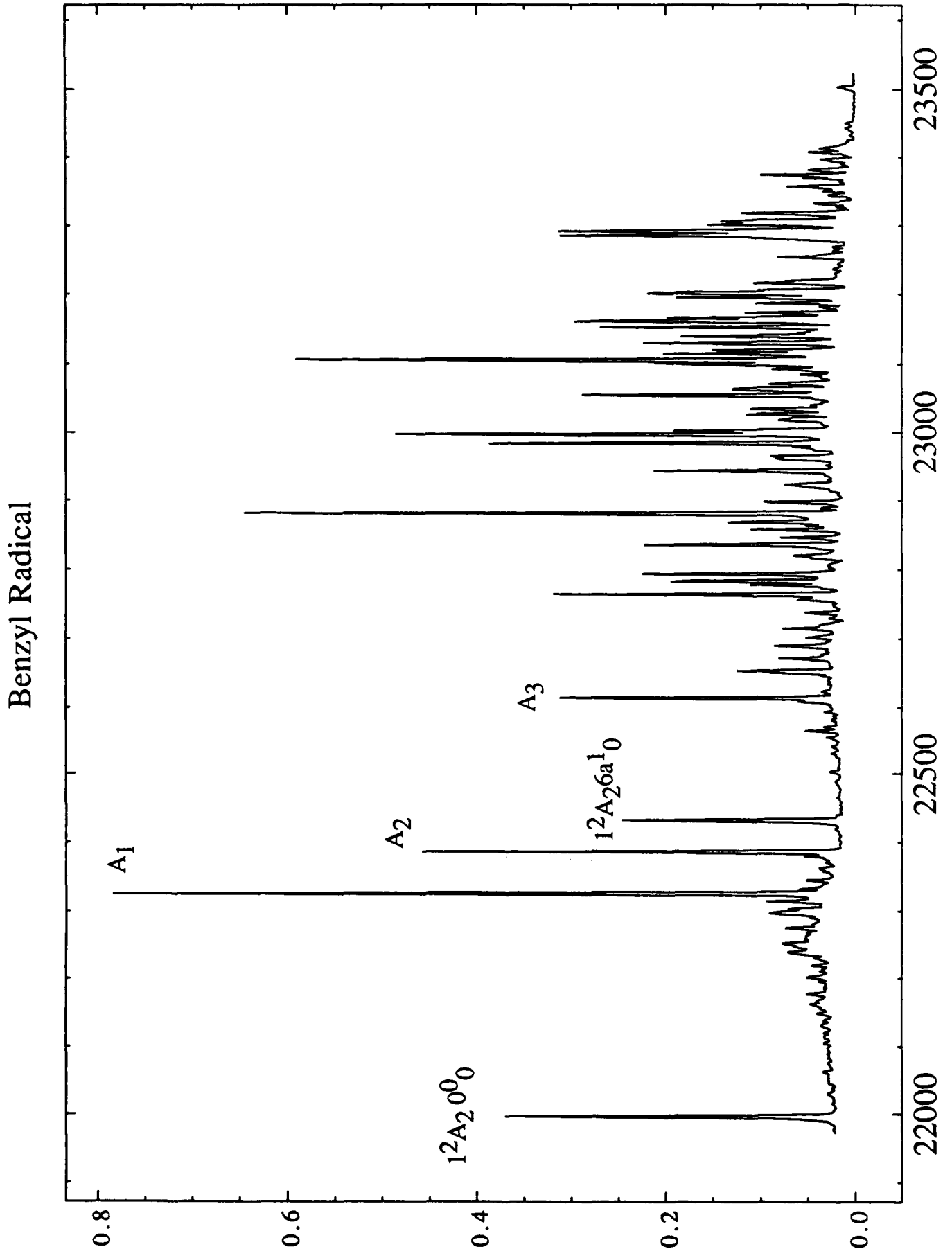
Benzyl Radical
A1
A2
A3
1²A2 6a¹ 0
1²A2 0⁰ 0
0.0
0.2
0.4
0.6
0.8
22000
22500
23000
23500
Wavenumbers (cm⁻¹)

Figure 3

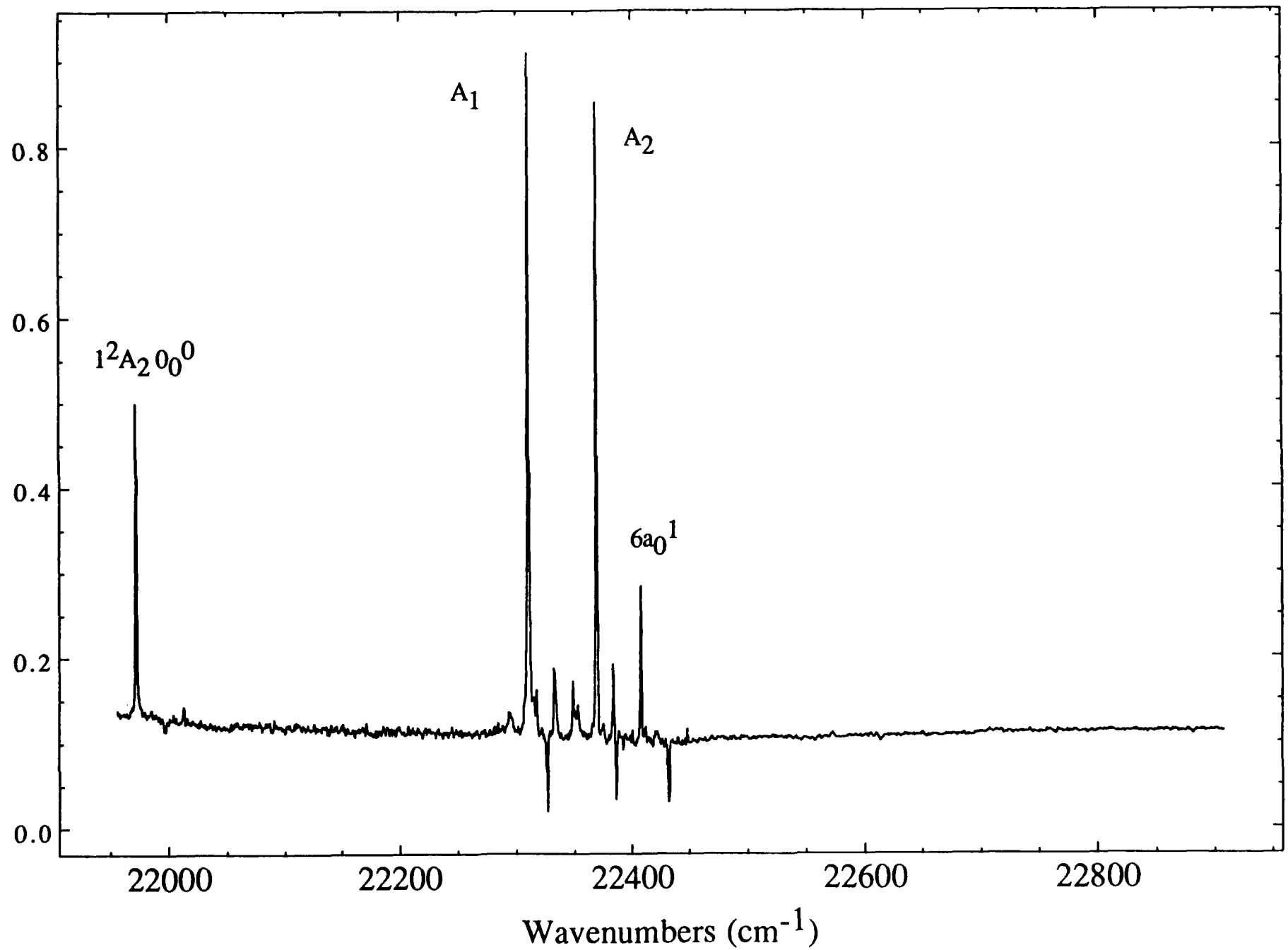
Benzyl Radical $(Ar)_1$
A_1
A_2
$1^2A_2\,0_0^0$
$6a_0^1$
0.8
0.6
0.4
0.2
0.0
22000
22200
22400
22600
22800
Wavenumbers (cm^{-1})

Figure 4

Benzyl Radical$(Ar)_1$

Top view

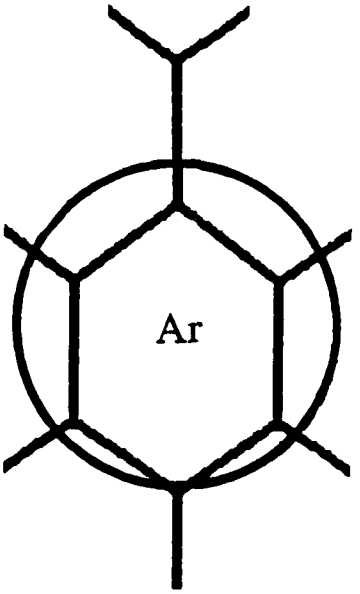

Side view

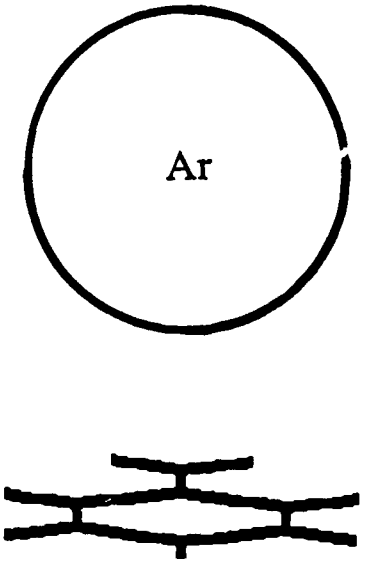

Figure 5

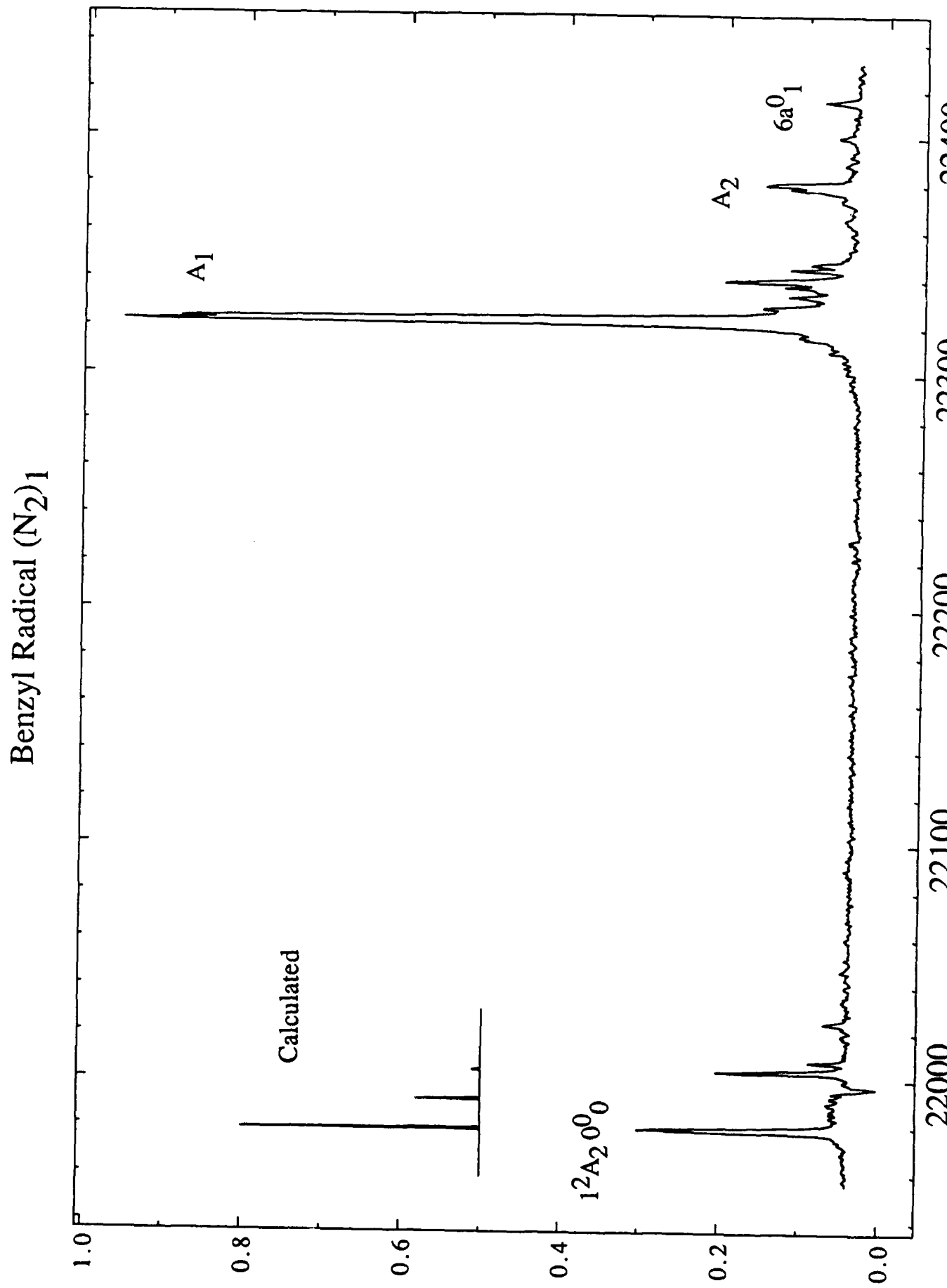
Benzyl Radical $(N_2)_1$
Calculated
$1^2A_2 0^0_0$
A_1
A_2
$6a^0_1$
1.0
0.8
0.6
0.4
0.2
0.0
22000
22100
22200
22300
22400
Wavenumbers (cm^{-1})

Figure 6

Benzyl Radical$(N_2)_1$

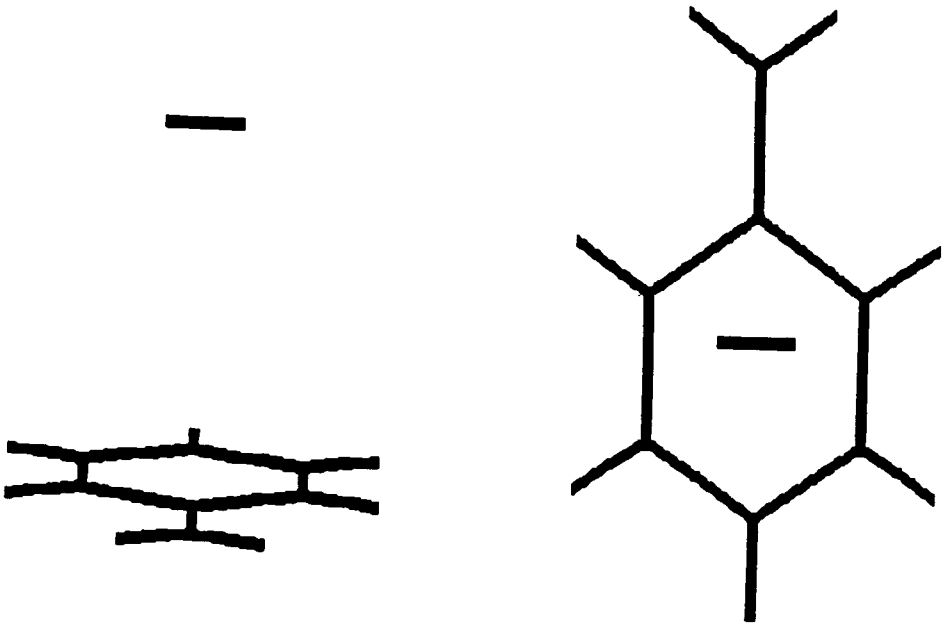

Side view 1^2B_2 Top view

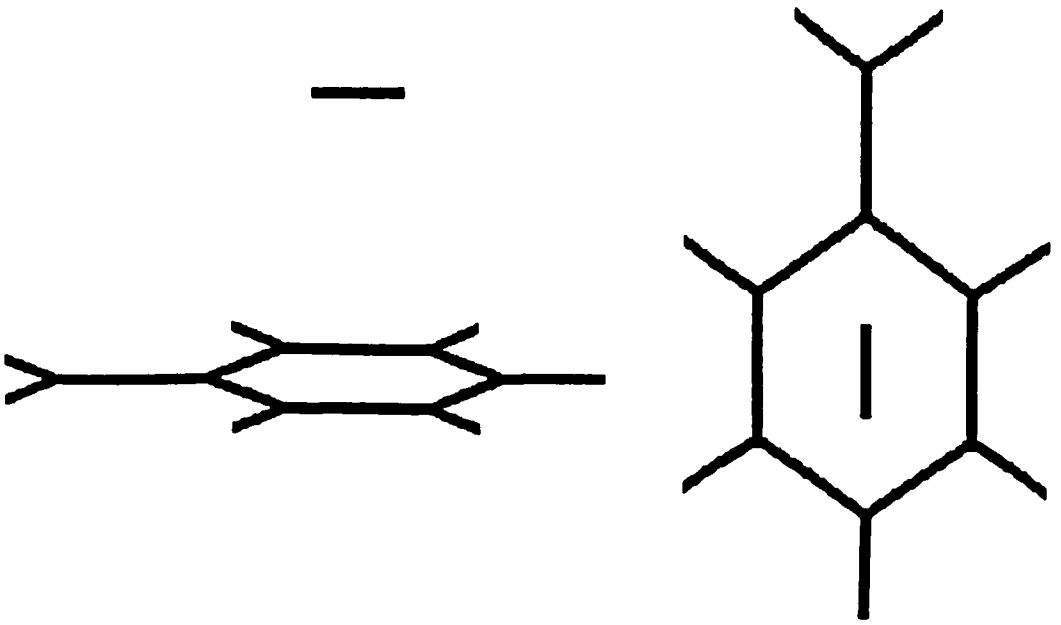

Side view 2^2B_2 Top view

Figure 7

Benzyl Radical $(N_2)_1$ D_0 and D_1 Translational Potential Energy Functions

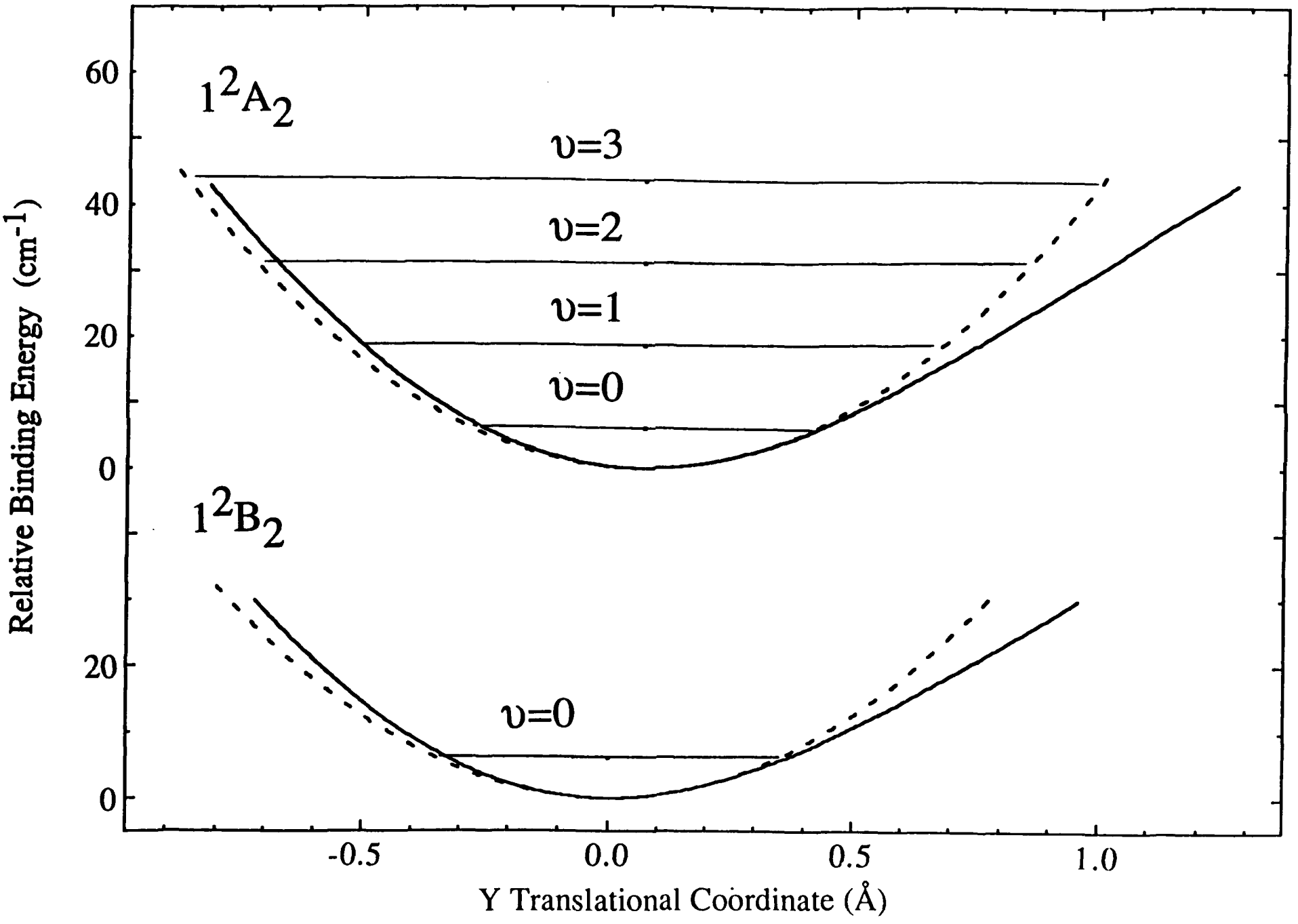

Figure 8

Benzyl Radical $(N_2)_1$ Rotational Potential Energy Functions

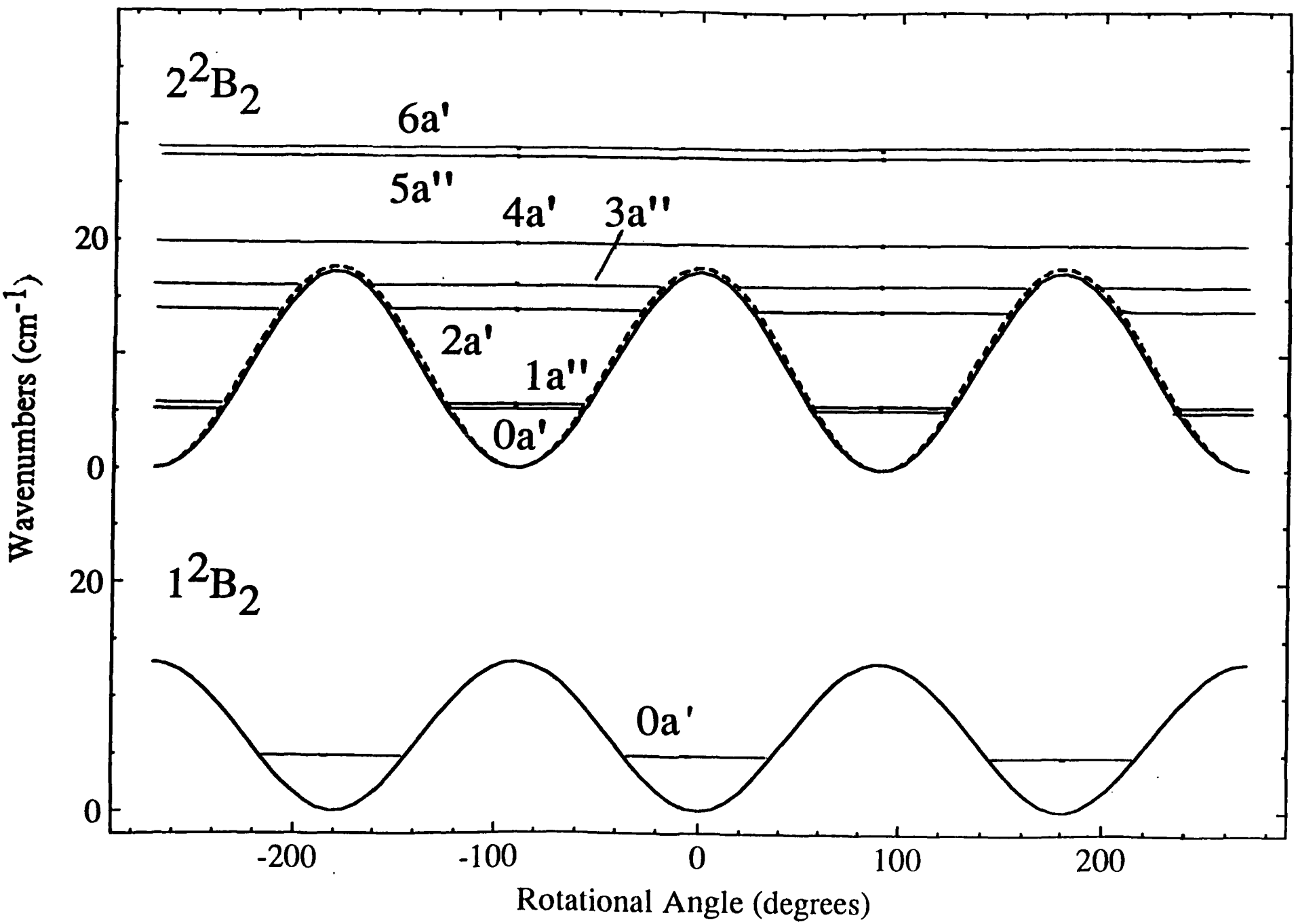

Figure 9

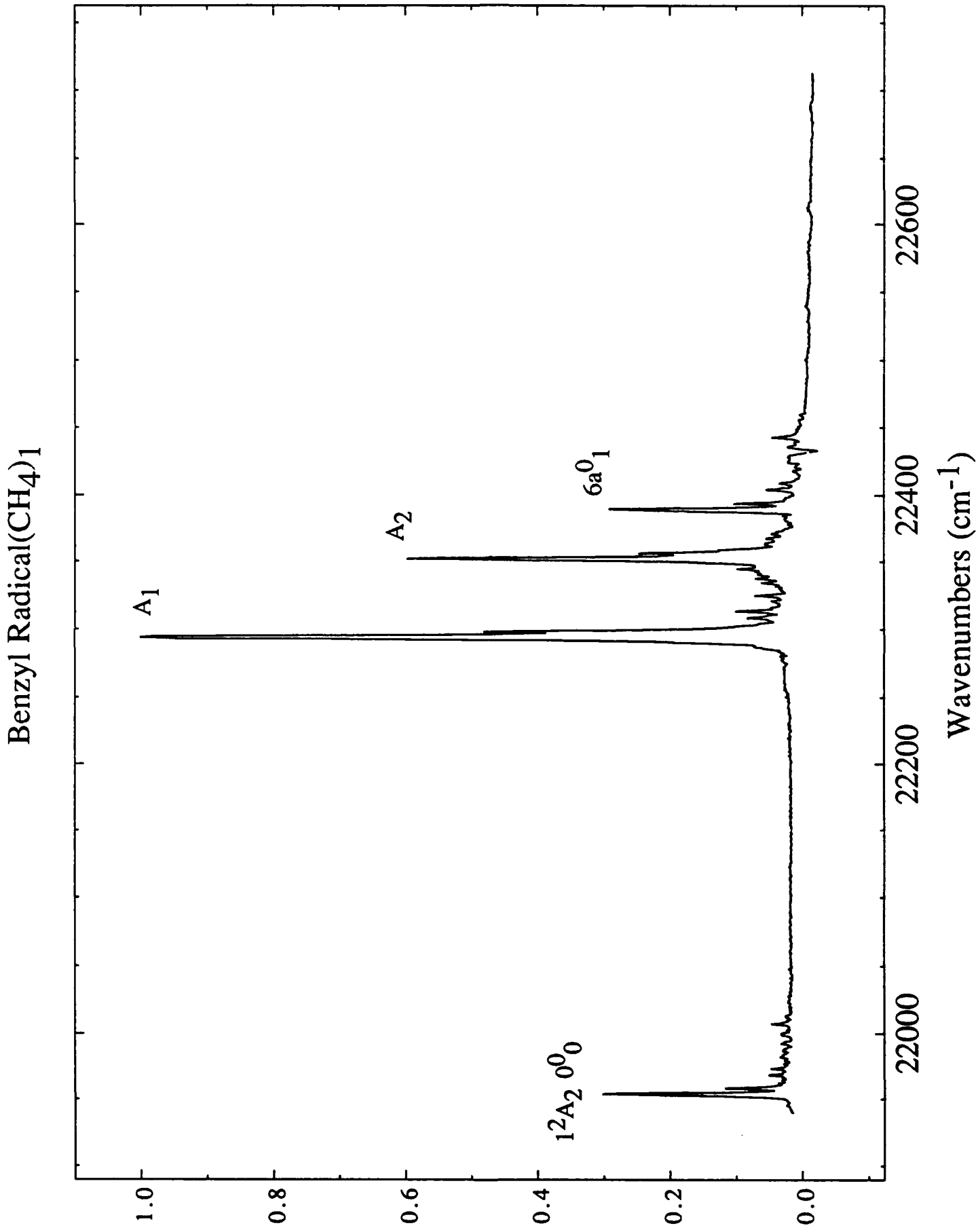
Benzyl Radical(CH4)1
A1
A2
6a0 1
1 2A2 0 0 0
1.0
0.8
0.6
0.4
0.2
0.0
22000
22200
22400
22600
Wavenumbers (cm-1)

Figure 10

Benzyl Radical$(CH_4)_1$

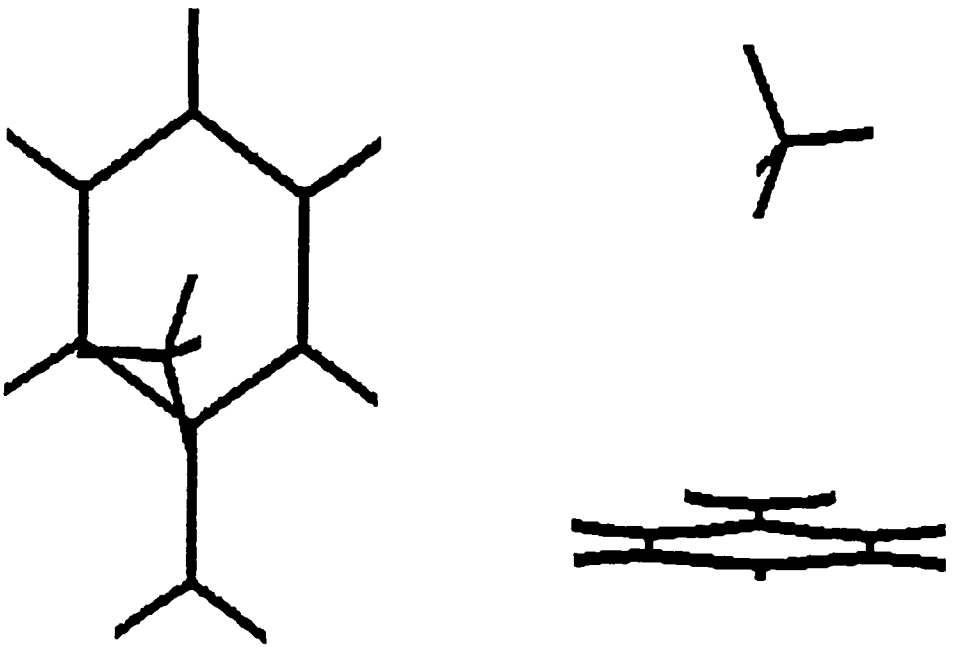

Top view Side view

1^2B_2 and 1^2A_2

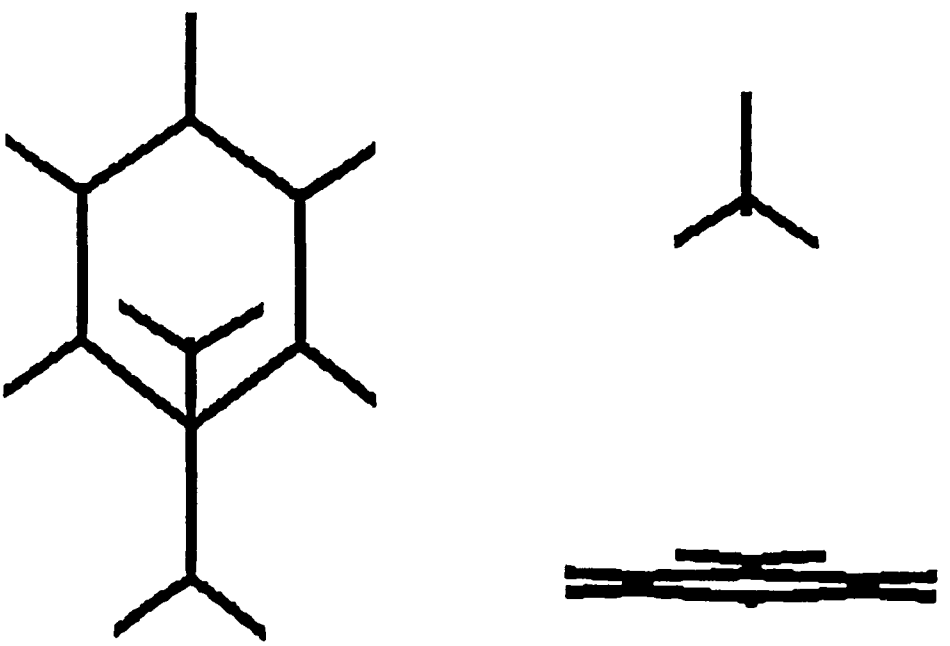

Top view Side view

2^2B_2

Figure 11

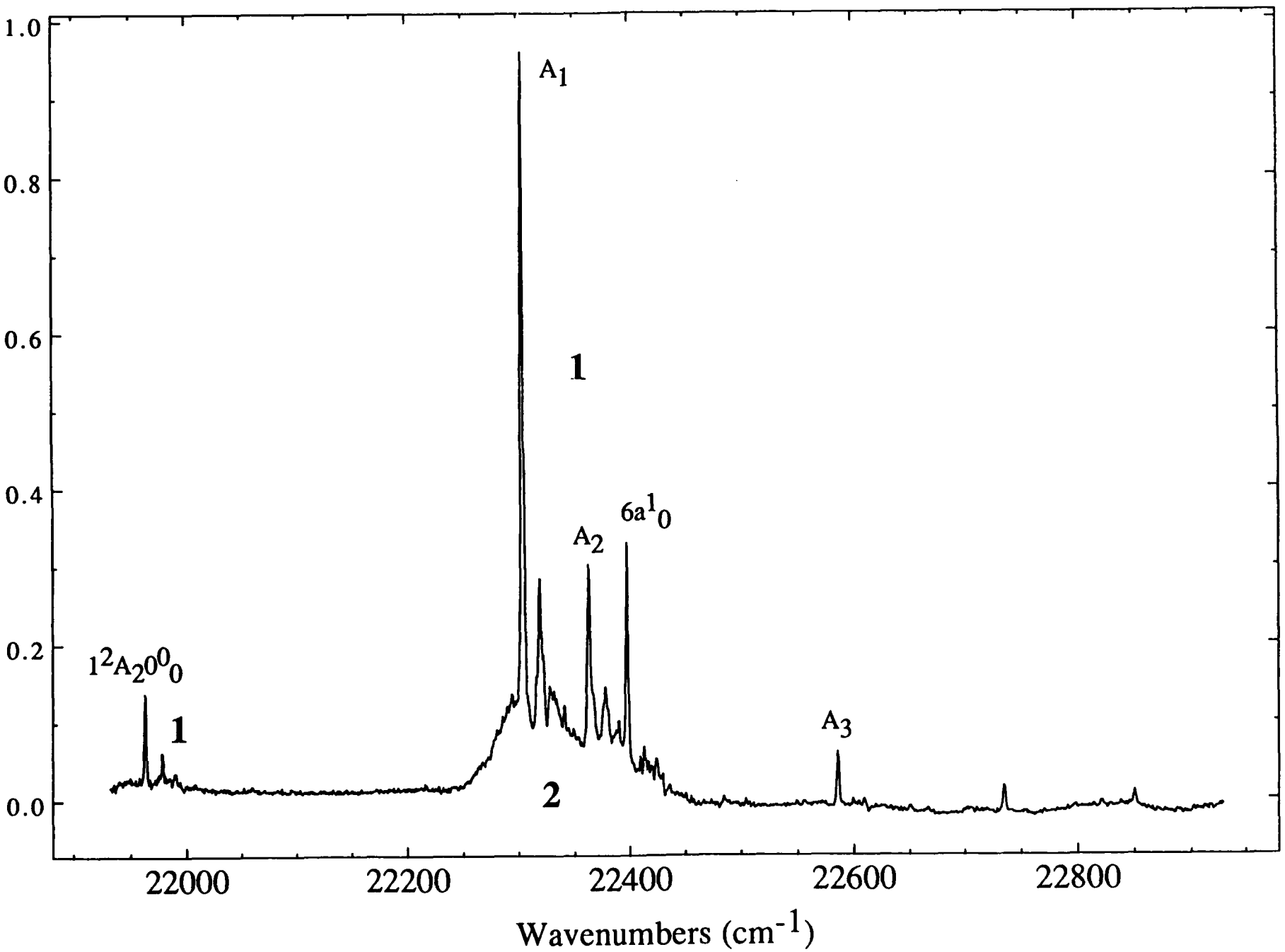
Benzyl Radical(C_2H_6)$_1$
1.0
0.8
0.6
0.4
0.2
0.0
A_1
1
$6a^1_0$
A_2
$1^2A_2 0^0_0$
1
2
A_3
22000
22200
22400
22600
22800
Wavenumbers (cm^{-1})

Figure 12

Benzyl Radical(C_2H_6)$_1$

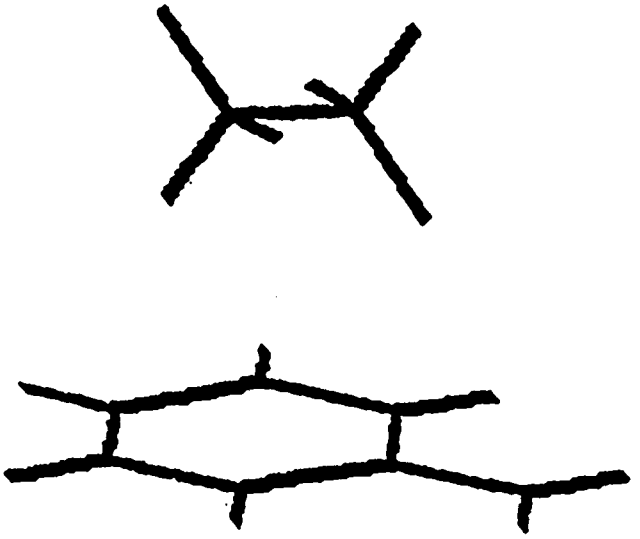

1

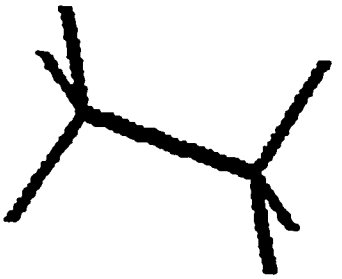

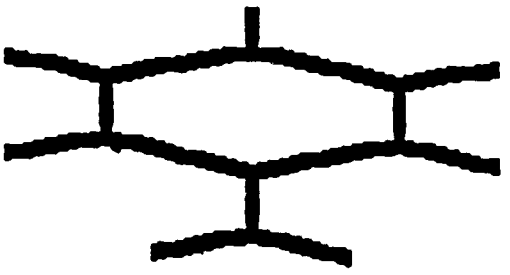

2

Figure 13

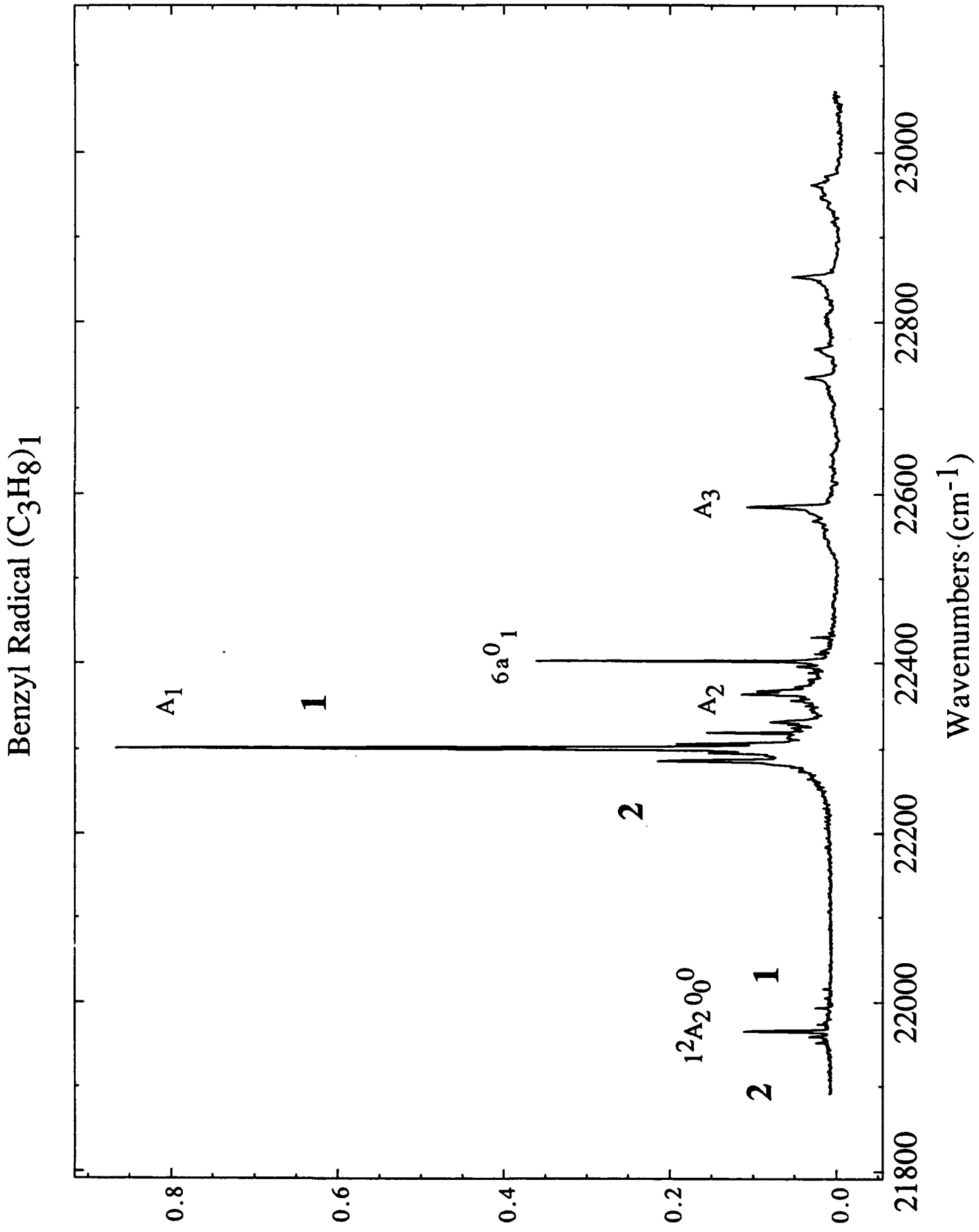
Benzyl Radical $(C_3H_8)_1$
A_1
1
$6a^0_1$
A_2
A_3
2
$1^2A_2 0_0^0$
1
2
0.8
0.6
0.4
0.2
0.0
21800
22000
22200
22400
22600
22800
23000
Wavenumbers (cm^{-1})

Figure 14

Benzyl Radical$(C_3H_8)_1$

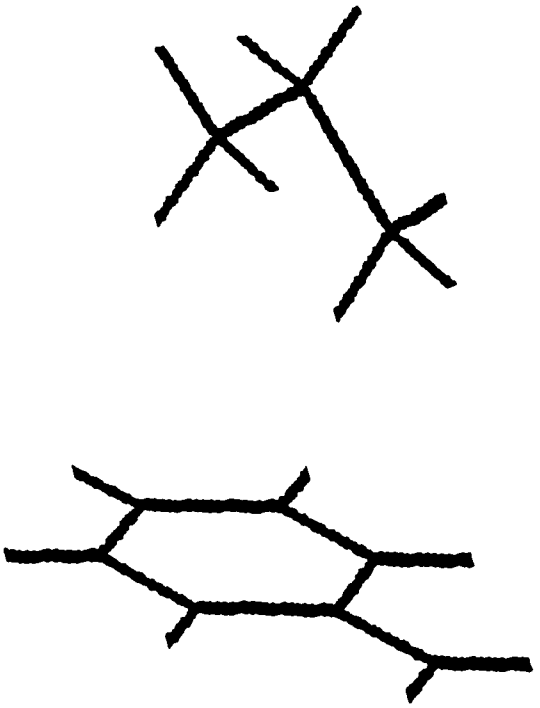

1

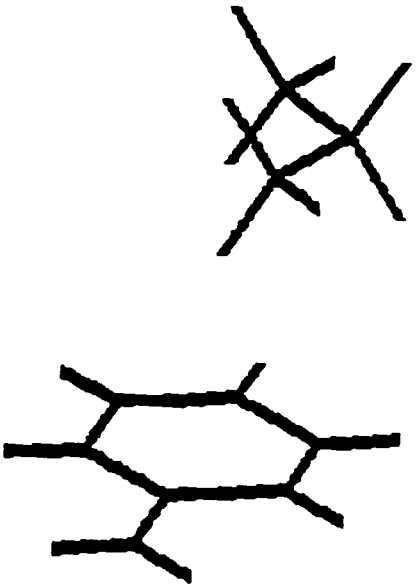

2

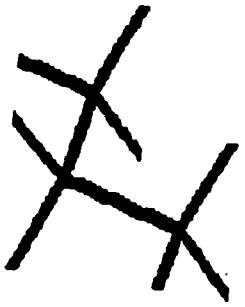

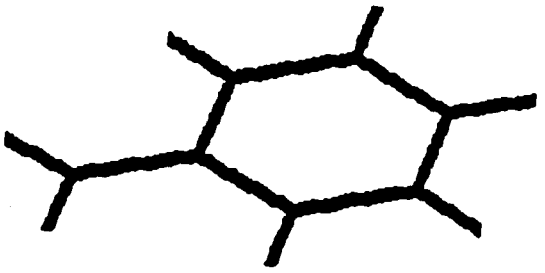

3

Figure 15